OPTICAL AND STRUCTURAL CHARACTERIZATION OF MIXED HALIDE PEROVSKITE THIN FILMS FABRICATED BY THERMAL CO-EVAPORATION

A THESIS SUBMITTED TO
THE GRADUATE SCHOOL OF NATURAL AND APPLIED SCIENCES
OF
MIDDLE EAST TECHNICAL UNIVERSITY

BY

ONUR YILMAZ

IN PARTIAL FULFILLMENT OF THE REQUIREMENTS
FOR
THE DEGREE OF MASTER OF SCIENCE
IN
PHYSICS

SEPTEMBER 2016

Approval of the thesis:

OPTICAL AND STRUCTURAL CHARACTERIZATION OF MIXED HALIDE PEROVSKITE THIN FILMS FABRICATED BY THERMAL CO-EVAPORATION

submitted by **ONUR YILMAZ** in partial fulfillment of the requirements for the degree of **Master of Science in Physics Department, Middle East Technical University** by,

Prof. Dr. Gülbin Dural Ünver ____________________
Director, **Graduate School of Natural and Applied Sciences, METU**

Prof. Dr. Sadi Turgut ____________________
Vice Chairperson of Department, **Physics, METU**

Prof. Dr. Raşit Turan ____________________
Supervisor, **Physics, METU**

Assoc. Prof. Dr. Selçuk Yerci ____________________
Co-Supervisor, **Micro and Nanotechnology Programme, METU**

Examining Committee Members:

Assoc. Prof. Dr. Alpan Bek ____________________
Dept. of Physics, METU

Prof. Dr. Raşit Turan ____________________
Dept. of Physics, METU

Asst. Prof. Dr. Selçuk Yerci ____________________
Micro and Nanotechnology Programme, METU

Asst. Prof. Emrullah Görkem Günbaş ____________________
Dept. of Chemistry, METU

Asst. Prof. Ayşe Seyhan ____________________
Dept.of Physics, Ömer Halisdemir Uni.

08.09.2016

I hereby declare that all information in this document has been obtained and presented accordance with academic rules and ethical conduct. I also declare that, as required by these rules and conduct, I have fully cited and referenced all material and results that are not original to this work.

Name, Last name: Onur YILMAZ

Signature :

ABSTRACT

OPTICAL AND STRUCTURAL CHARACTERIZATION OF MIXED HALIDE PEROVSKITE THIN FILMS BY THERMAL CO-EVAPORATION

YILMAZ, Onur

M.S., Physics
Supervisor: Prof. Dr. Raşit Turan
Co-Advisor: Assoc. Prof. Dr. Selçuk Yerci
September 2016, 82 pages

Cost-effective, easy-to-produce, optically and electrically configurable properties of perovskite allow researchers to perform a profound investigation to better understand its physical and chemical nature. Additionally, band gap tunability by introducing bromide (Br) to replace iodine (I) also makes perovskite a suitable material for tandem solar cells. However, to fully benefit from perovskite cells, hysteresis in current-voltage curve, poor stability and relatively low fill factor in large area devices need to be overcomed. In the literature, various deposition techniques (spin coating, dip coating and thermal evaporation combined with one of the first two) have been used for fabricating Br containing perovskite. In this thesis, mixed halide ($CH_3NH_3PbI_{3-x}Br_x$) perovskite thin films were fabricated entirely by thermal co-evaporation in the full range (x is ranging from 0 to 3) for the first time. Five sets of samples having different Br/I ratio including two extremes (only iodide and only bromide containing) were fabricated successfully after achieving high crystallinity and uniform morphology by optimizing the deposition conditions. Perovskite films with different Br/I ratio were characterized optically and structurally using photoluminescence, X-ray diffraction, reflection and transmission, and scanning electron microscopy measurements. The results clearly demonstrate band gap widening and lattice constant increase with Br concentration. $CH_3NH_3PbI_2Br$ sample with a band gap of 1.65 eV, suitable for tandem solar cells were fabricated with no Stokes shift in PL .

Keywords: perovskite, co-evaporation, bromide, band gap tunability

ÖZ

TERMAL EŞ-BUHARLAŞTIRMA İLE ÜRETİLEN KARIŞIK HALOJENLİ PEROVSKİT İNCE FİLMLERİN OPTİK VE YAPISAL KARAKTERİZASYONU

YILMAZ, Onur

Yüksek Lisans, Fizik
Tez Yöneticisi: Prof. Dr. Raşit Turan
Tez Eş-Yöneticisi: Yard. Doç. Selçuk Yerci
Eylül 2016, 82 sayfa

Perovskitin uygun maliyetli, üretimi kolay, optik ve elektriksel özelliklerinin ayarlanabilir bir malzeme olması araştırmacıların perovskitin fiziksel ve kimyasal özelliklerini daha derinlemesine araştırmasına olanak sağlamıştır. İyot (I) yerine brom (Br) kullanılarak bant aralığı ayarlanabilir olması perovskiti tandem güneş hücreleri için uygun bir malzeme yapmaktadır. Ancak, perovskit güneş hücrelerinden tamamen yararlanabilmek için, akım-voltaj eğrisindeki gecikmeler, zayıf kararlılık, ve geniş alan hücrelerdeki görece düşük doluluk oranının üstesinden gelinmesi gerekmektedir. Farklı üretim teknikleri (spin kaplama, daldırarak kaplama ve ilk ikisiyle birlikte olacak şekilde termal buharlaştırma) Br içerikli perovskit üretimi için denenmiştir. Bu tez çalışmasında tamamen termal eş buharlaştırmayla karışık halojenli perovskit ($CH_3NH_3I_{3-x}Br_x$) ince film tüm bant aralığında (x değeri 0'dan 3'e kadar) ilk kez üretilmiştir. Film kristalinitesi ve yapısı iyileştirilerek iki uç nokta da dâhil (sadece iyodür ve sadece bromür) farklı Br/I oranına sahip beş takım örnek başarıyla üretilmiştir. Farklı Br/I oranına sahip perovskitlerin optik ve yapısal incelemesi fotolüminesans, X ışını kırınımı, yansıma, geçirgenlik, taramalı elektron mikroskopu ölçümleri kullanılarak yapılmıştır. Sonuçlar açıkça Br oranıyla bant aralığının ve örgü aralığının artığını göstermektedir. 1.65 eV bant aralığına sahip tandem uygulamalar için uygun $CH_3NH_3I_2Br$ örneğinde Stokes yer değiştirmesi gözlenmemiştir.

Anahtar kelimeler: perovskit, eş-buharlaştırma, bromür, bant aralığı ayarlanabilirliği

Dedicated to the dream followers we lost in Suruç…

ACKNOWLEDGEMENTS

I would like to thank my co-supervisor Assoc. Prof. Dr. Selçuk Yerci for his guidance and patience during my thesis study. He has given me another chance to complete what I started.

I would like to thank Prof. Dr. Raşit Turan for his supervising and all the GÜNAM employees and members giving me technical support during my experiments.

I would like to thank all the people in APP group. Especially, I am very grateful for all the help and good conservations with Wiria, without his help I could not make it all the way. I am also thankful to Cem Şahiner who has been also helpful and always cool and calm with his deep knowledge about the chemistry.

I would like to thank my family and for their understanding, moral and financial support during my thesis study.

Throughout the whole time I spent at METU outside physics courses, I have learnt important lessons about life. All the memories are very precious for me as they shape me who I am today. From the moment I stepped in to the last days, I am grateful to all the people who I share the same ideals for the world and the future. Mentioning some of the names here at least that I can do. I appreciate the camaraderie of Elif Nur Yaman, Yoldaş Aydın, Seçkin Şiş, Ozan Özgenler, Berfum Çolak, Irmak Sel, Volkan Muyan, Melis Çevik, Alican Uçarcan and so on.

It is not enough to describe the importance of Cansu Yumuşak in my life with the words here. She is the most influential person of my life. Meeting with my friend and my love changed my life more than being here and studying physics. I am thankful to her, especially for her patience and endurance during the time of writing.

This thesis work was supported by the Scientific and Technical Research Council of Turkey (TUBITAK) under the contract number 114F306. I also would like to thank TUBITAK for 2210 scholarship program as the financial support during my master of Science.

TABLE OF CONTENTS

CHAPTERS

LIST OF FIGURES

FIGURES

LIST OF SYMBOLS

Symbol	**Description**	**Unit**
MAX	Methylammonium Halide	-
PbX_2	Lead Halide	-
Å	Angstrom	10^{-10} m
α	Absorption Coefficient	cm^{-1}
λ	Wavelength	nm
d	Thickness	cm
R	Reflectance	%
T	Transmittance	%
θ	Incident Angle	degree (˚)
n	Diffraction Order	-
h	Planck’s constant	4.136 eV*s
ν	Frequency	1/s
E_g	Band Gap Energy	eV

LIST OF ABBREVIATIONS

CPU	Central Processing Unit
DSSC	Dye-Sensitized Solar Cells
EDX	Energy Dispersive X-Ray Spectroscopy
FWHM	Full Width Half Maximum
LED	Light Emitting Diode
MA	Methylammonium
MABr	Methylammonium Bromide
MAI	Methylammonium Iodide
PCE	Power Conversion Efficiency
PID	Proportional-Integral-Derivative
PL	Photoluminescence
PPM	Particle Per Million
PSC	Perovskite Solar Cell
PV	Photovoltaics
RoHS	Restriction of Hazardous Substances
QCM	Quartz Crystal Microbalance
SEM	Scanning Electron Microscopy
TE	Thermal Evaporation
UPS	Ultraviolet Photoelectron Spectroscopy
WEEE	Waste Electric and Electronic Equipment
XPS	X-Ray Photoelectron Spectroscopy
XRD	X-Ray Diffraction

CHAPTER 1.

INTRODUCTION

1.1. Motivation

The modern life is evolving around the energy. New technologies and all the new life-changing inventions bring their own ever accelerating energy demand. Our life style is so energy dependent that even the basic services cannot be done without an energy source. However, the planet cannot tolerate the outcome of our energy exploitation anymore. The accumulation of the reckless energy for the last 200 years brings out a huge crisis for the whole life on earth. Climate change is threatening not the future generations only, it exists now and affects the present time. Extinction seems inevitable for some species. For mankind, thousands of people have already lost their lives and those who survive are climate refugees now. Millions of lives who live in fragile areas with extreme climate conditions are in danger. Life is unbearable on earth right now for millions of people while rest of them still try to figure out the magnitude of this issue. Up to now, most of the people do not take climate change as serious as it is. The very existence of the civilization built for centuries is about to collapse with the decisions of the ones who are building it. We need an emergency plan to save the planet and the life. Scientific research can make this plan. After all, the cause of it is a result of scientific progress in some aspect, but with a misleading political program. It is about the time to decide that this plan is either to be a rescue plan or a transition plan. Science keeps the hopes for this transition by bringing a solid basis of how it should be. It is time for a permanent transition towards a more ecological life without giving up the current life quality.

One of the solid reasons of climate change is the way we produce the energy. That is why renewable energy sources are the key parameter for a universal solution. The urgency of the situation dictates us to start with the energy sources and energy policies to create a chance to overcome. Today, fossil fuel dependent economy dominates the energy policies. Economical superiority of fossil fuels is not only related with their energy efficiency. It is also related with the market system of energy production. For the last two years, oil prices are going down and that is all the needed for a sustainable economic growth. The energy policies are unquestionable if the market keeps its profitability.

Although the costs are now competent for some applications, there are still enormous fossil fuel investments going on around the world. Market perspective does not have a sense for sustainability of the nature or the future. Economy based approach dragged the world into a massive crisis and climate change makes it crystal clear that we need to change this energy perspective for our future. However, it is not only scientifically shown that it is too late for a total mentality change, but also catastrophic events prove the opposite every day. The energy sector acts slowly as CO_2 emissions are projected to be 16% higher by 2040 although it plays a central role to overcome climate change [1]. To act towards the core of the issue, implementing renewables can be a starting point. To do that, cost reduction seems to be the key parameter. Low cost material research is top-notch priority especially for renewable energy.

In this aspect, perovskite is promising material for the future. The perovskite research has just taken off, but the outcomes already attract the energy sector players despite the commercialization questions around it. This study can be considered as a minor contribution to this effort to make the earth livable again for everyone.

1.2 Lead Halide Perovskite

Discovery of $CaTiO_3$ by Gustav Rose in 1839 who named the mineral after Russian mineralogist Lev Perovski introduced a new kind of material to the science. Perovskite then became the name of compounds having the composition ABX_3, the same crystal structure as $CaTiO_3$. Although it is known for decades, it has not become an intriguing material until the researchers focused on a particular type of organic-inorganic hybrid perovskite in the early 90's [2] [3] [4] [5]. These materials incorporate a cation which is commonly organic such as methylammonium (MA) or formamidinium (FA) on the A site and a divalent metal such as lead (Pb^{+2}) and tin (Sn^{+2}) on the B site. The metal ions are octahedrally coordinated by 8 halide anions (Cl^-, Br^-, I^-) on the X site.as shown in Figure 1.1.

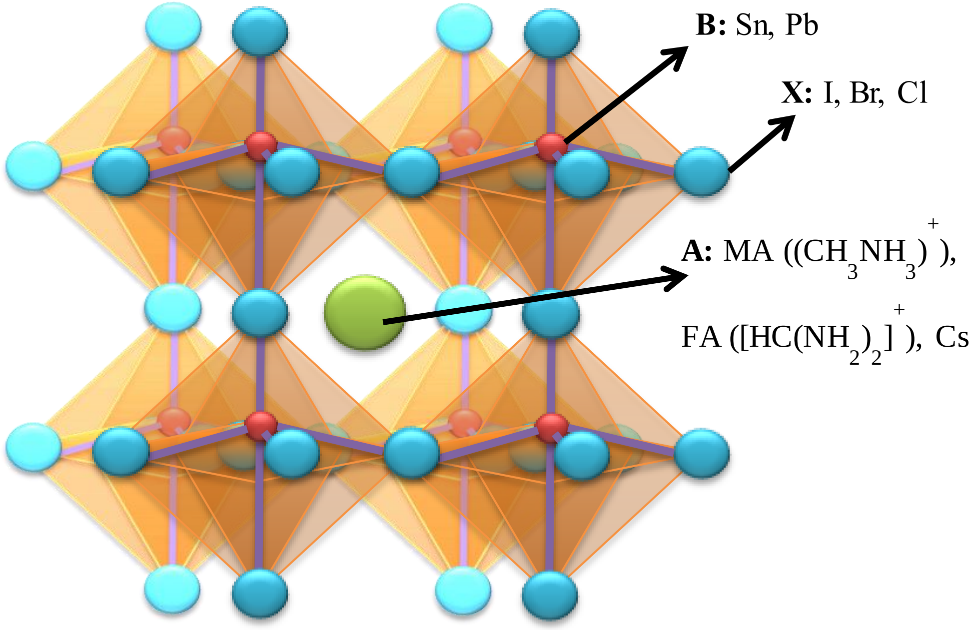

Figure 1.1: Ideal ABX_3 perovskite structure and commonly used materials

In perovskite structure shown in Figure 1.1, sizes of sites determine the crystal phase of perovskite. Si, GaAs, CIGS, CdTe solar cells are generally constructed with tetrahedral semiconductors while perovskite is more cubic with heavier atoms like Pb and I in its structure [6]. If cation A is slightly small, less symmetric orthorhombic structure forms. At low temperatures, all perovskites of interest in these applications form orthorhombic phase. More symmetrical phases occur with increasing temperature until cubic structure is formed generally around room temperature. Organic cations at site A do not have a spherical shape; rather they have fixed orientations for the low temperature at orthorhombic phases within the unit cells. However, they oscillate between different positions for higher temperature phases on a picosecond time scale, and form a spherical symmetry on average [6].

Perovskite is mainly studied due to their easy synthesis and interesting optoelectronic properties [7] [8]. Thin film transistors and light emitting diodes (LED) was studied in earlier researches [9] [10]. High absorption coefficient, long minority carrier lifetime, low Urbach energy, high PL quantum yield, low exciton binding energies, low effective masses, the presence of only shallow defects in the band gap and tunability of the band gap of the perovskite moved the focus of the research into solar cell applications later [11-20]. These properties draw a great attention for both single junction and tandem applications [21] [22]. Band gap tunability and low temperature deposition allow perovskite as top sub-cell with Si, CIGS and CdTe as bottom sub-cell [23-27].

From UV range to near IR region, $MAPbX_3$ perovskite band gap can be tuned over hundreds of nanometers by modifying organic, metallic and halide sites chemically [28-30]. Reddish colored emission from $MAPbI_3$ LED's shifts to green when gradually substituted with Br [31]. Adding Cl to $MAPbBr_3$ perovskite LED's changes the green color to blue by widening the band gap even further. Perovskite film colors also shift from dark brown to brown/red, then from orange/yellow to colorless transparent by mixing I with Br and Br with Cl [32]. However, I-Cl compositions do not change the band gap as Cl atoms do not take part in the crystal structure because of the large difference between I and Cl atomic sizes [12]. Perovskite is a rare material in that sense by tunable semitransparency as keeping its device efficiency at a considerable value. Transparency of the films comes from the morphology of perovskite. Grain sizes reach to micrometer level which can absorb the visible light sufficiently while the gaps between the grains allow transmission depending on the thickness of the film [33].

The working mechanism of perovskite is under investigation more intensely after losing the momentum in record breaking devices recently. Perovskite's relatively small grains compared to other semiconductors make it more intriguing how it actually works in these high efficient devices. It is debated which charge carrier type perovskite has to get more insight about its electrical properties. For direct band gap semiconductors like perovskite, bound excitons and free electron-hole pairs are two possible photo-products. Magnitude of Coulomb attraction screened by the dielectric properties of perovskite determines which one will be the charge carrier type [34]. The Elliot theory explains the absorption phenomena near the band gap in direct semiconductors [35]. Exciton binding which is also dependent on the dielectric property is the main parameter for understanding the dominant species. Structures of solar cells are modified according to this carrier transport mechanism of the semiconductor. Free carrier based solar cells have internal electric field for extraction of holes and electrons, meaning a homojunction is suitable to create a current while bound exciton based devices such as organic solar cells need heterojunctions for splitting the positive and negative carriers. Considering the different structure types of perovskite solar cells (including the ones with both transport layers, no hole transport layers or inverted structured ones), it can be concluded that excitons and free carriers can co-exist in perovskite and the working mechanism depends on the device structure [36]. Long carrier diffusion length of perovskite can be related with free carrier dominated cases while smaller values represent the excitonic case. Binding energy of perovskite is at intermediate values. Thus, without further characterization, it cannot be defined as excitonic or free carrier-based and results show that they exist simultaneously shown in Figure 1.2.

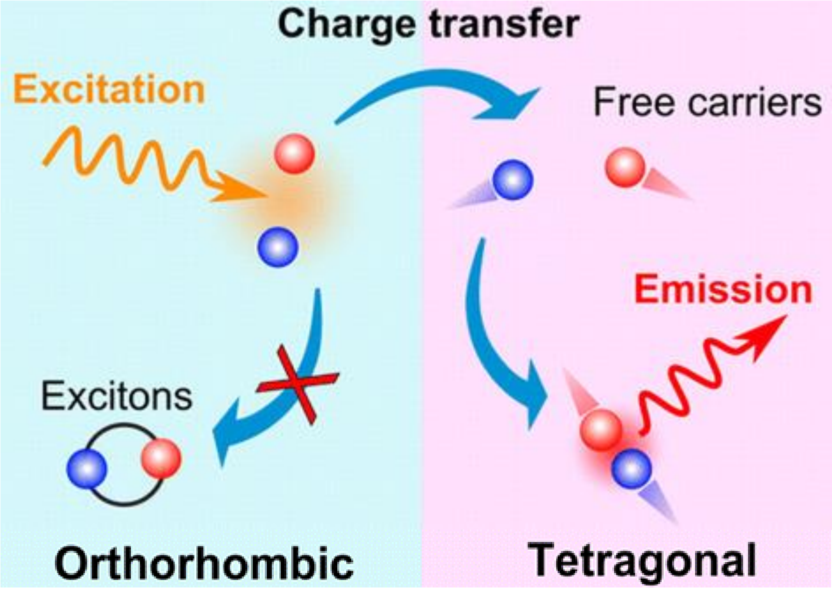

Figure 1.2: Co-existence of free carriers and excitons in perovskite [37]

For the commonly used $MAPbI_3$ perovskites, emissions are mainly generated from band to band transitions and its radiative efficiency is 200 times higher than organic solar cells. Hence, open circuit voltage is closer to its theoretical point. Photoluminescence is weaker at short circuit than for open circuit conditions indicating free carriers with small binding energies [34]. Another proof of free carriers for $MAPbI_3$ perovskite under steady illumination shows that charge density ($1.4 \pm 0.12 \times 10^{15}$ cm^{-3}) is an order of magnitude higher than measured by Hall Effect. This amount of carrier density means the photo-products are free carriers [36]. For mixed halide perovskite, these values vary since the band gap formation of these defined by Pb and halide ions which alter the dielectric properties. Organic cation, on the other hand, do not affect the electronic properties since its valance band are deeper than the overlapped Pb and halide ion valence bands [37]. Temperature also changes the working mechanism of perovskite. At room temperatures, optical transition peaks of two species are indistinguishable while excitonic peak is more pronounced for lower temperatures down to 170 K [36].

Perovskite was first used as a replacement of dye in the dye-sensitized solar cells (DSSC) in 2006 with power conversion efficiency (PCE) of 2.2%. In 2009, mixed halide trial by using Br was report with PCE of 3.8%. First perovskite solid-state solar cells were reported in 2012 [13]. After regaining its popularity with solar cells, novel LED and laser application are boosted [34-36]. Commercial solar cells which have been studying over 40 years, passed the 20 % efficiency milestone after decades; but perovskite solar cell efficiency was already above 20% after three years as shown in Figure 1.2. Astonishing progress for 3rd generation solution-processed PV technologies was achieved with lead halide perovskite solar cells.

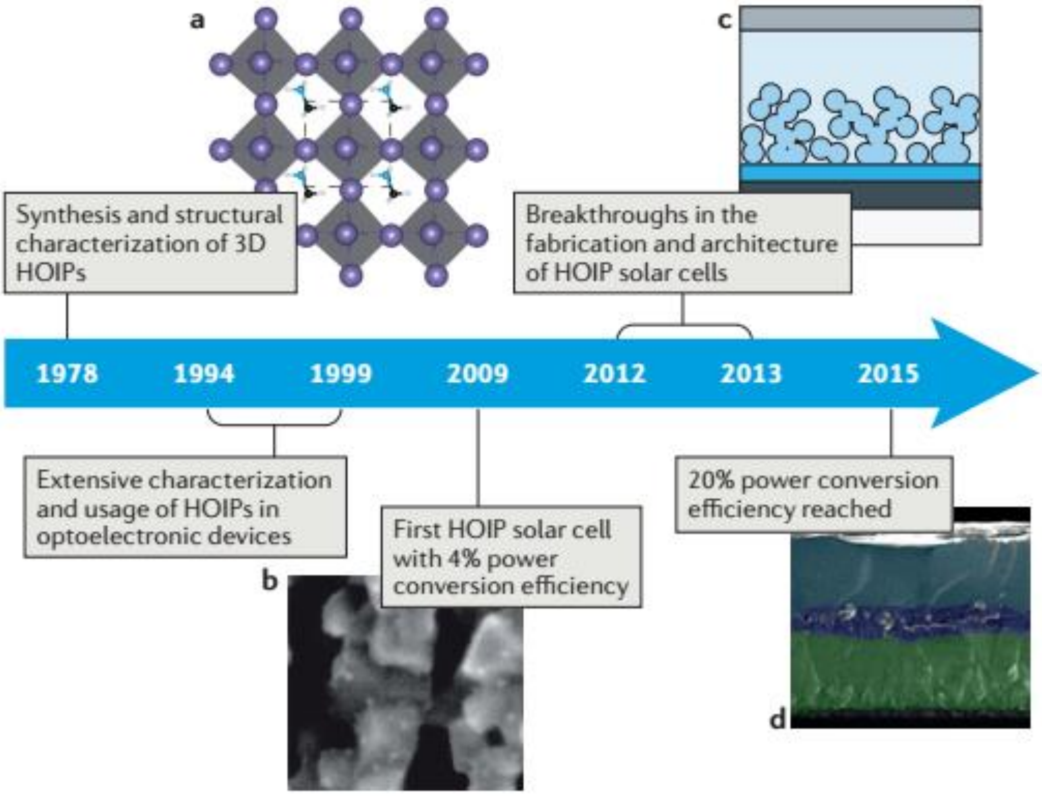

Figure 1.3: Timeline of perovskite research with important milestones [41]

Perovskite seems a perfect semiconductor for PV applications with its optoelectronic properties. However, three main challenges are present against its commercial use: stability and scalability of devices and its use of lead.

Relatively high humid, temperature and high intensity UV light create instability in perovskite structure [42-44]. These effects also limit the carrier mobility including halide ions which can contribute the working mechanism of devices [45]. More stable perovskite solar cell performances are achieved with different device structures. After over 1000 hours of degradation tests, 80% of the initial efficiency is measured [46]. There are various studies to define the exact reasons of instability and degradation. Each study focuses on different degradation pathways and completes the full mechanism of perovskite instability. Chemical changes in surface and bulk of perovskite film, structural and phase changes, thermal and mechanical properties are studied both experimentally and theoretically for this purpose [47]. Main difference between perovskite and other traditional materials used in PV devices is that the properties of perovskite do not remain same after illumination and measurements. Moreover, the content of perovskite is also a parameter how the ambient conditions affect the degradation process. $MAPbI_3$ perovskite films degrade at humidity over 50% while $MAPbBr_3$ do not. By using tunability property, mixing these two halides for x=0.20 and 0.29 in $MAPb(I_{1-x}Br_x)_3$ enables a 20 days of stable perovskite [48]. This is resulted from more stable structure. Replacing smaller size Br atoms (1.96 Å) with I atoms (2.2 Å) reduce the lattice constant and transition to cubic phase occurs [47] [49]. Tetragonal phase (I4/mcm) of $MAPbI_3$ transits to cubic phase (Pm3/m) which is more symmetric [32]. Adding Cl alongside with Br also improves the stability of the perovskite [32] [50].

Photo-induced instability, unlike humidity, cause reversible changes in perovskite. It was shown that in mixed halide perovskite films, ion migration create phase segregation. XRD peaks of $MAPb(I_{1-x}Br_x)_3$ films split when illuminated for long times and merge back to original position when left in the dark [51]. Although this ion migration property can be useful for specific applications, it results in hysteresis in the devices which is independent from light intensity [52]. Mixed halide solar cells exhibit poor performance compared to $MAPbI_3$ used devices. Most probable reason is considered to be this phase separation. Earlier studies demonstrate the formation of deep traps in iodide rich areas causing voltage loss [53]. Halide mixing was studied comprehensively including characterizations of optical and structural properties. PL measurements confirm the ion migration. There appears a new peak at ~1.68 eV other than original peak of perovskite. This new peak position is independent from starting Br content, only for less than 20% Br incorporation, it needs longer illumination. This PL anomaly is also parallel with XRD results which sharp peaks of original perovskite split upon illumination [54]. $MAPbX_3$ based perovskite films undergo a phase transition around 50℃ which is around the operating range of solar panels in summer time [55].

Methylammonium lead halides are the most commonly used perovskites in highest efficient devices. The amount of lead in the final PV module may be low comparing with other lead used applications, but the regulations limit its use even for this extent. The lead content of a 300 nm thick $MAPbI_3$ absorber is calculated as 0.3 g/m^2 which correspond to 120 ppm Pb on 2.5 kg/m^2 module made on 1 mm thick glass [56]. The laws for electrical products within Europe such as WEEE (Waste Electrical and Electronic Equipment) and RoHS (Restriction of Hazardous Substances) allow this amount of lead used in PV modules. However, for consumer products, the laws would apply for these amounts even with a good encapsulation [57]. A waterproof encapsulation has not yet been passed the stability tests for long hours like Si PV modules which are guaranteed for over 20 years. Same development and technology deployment may not be applied for perovskites, thus further research on toxicity and stability is needed.

1.3 Research Aim

Renewable energy research focuses on clean technologies to make a significant change on carbon emissions and thin film photovoltaics play a crucial role in this regard. Although perovskite films are fabricated from abundant, low-cost elements, it is unlikely to compete with the prices of state-of-art PV technologies on its own. Process and material cost reductions do not have the biggest impact on electricity/cost (W/TL) value. It is actually the device efficiency that reduces the cost/efficiency value most by also lowering the installation, housing and assembly costs [58]. Thus, perovskite solar cells are first aimed to enhance the current technology performances. Increasing the efficiency with tandems reduces the sizes of modules needed for the desired power. To exceed the Shockley-Queisser limit of single junction solar cells (33.7%), double junction tandems (theoretical efficiency limit of 46.1%) can be introduced. Perovskite is an incentive top sub-cell candidate as mentioned in previous section. $MAPbI_3$ absorber with 300 nm thickness costs less than 2 dollars/m^2 with easy coating processes by cheaper equipment compared to Si based modules [59]. Cost effective solution process fabrication requires minor upgrades for manufacturing equipment while it has fundamental constraints.

In this thesis, one of the main challenges for tandem applications, band gap tuning is aimed to be achieved by thermal co-evaporation (others can be photon management, transparent electrodes and parasitic absorption of other layers) [27]. Ideal band gap for 1.12 eV band gap bottom Si sub-cell range from 1.65 to 1.9 eV depending on where it is installed and can give around 40% efficiency at its best [60] [61]. Br-I mixing to get this band gap range can result in sub-band gap absorption and modified techniques are needed to overcome [48]. One step solution process, sequential two step deposition process, spray coating, slot-die coating, sequential vapor deposition, vapor-assisted solution process, blade coating, flash assisted deposition are other techniques used for perovskite fabrication. Thermal co-evaporation has better thickness and morphology control among others. Downside of thermal co-evaporation is redefining the evaporation rates and optimizing the system parameters such as pressure. Organic source salts used in thermal evaporation can also cause some problems regarding its sublimation temperature stability [62]. Other than lattice mismatch and possible high temperature steps of device fabrication, reproducibility of the same band gap perovskite by solution processes can be challenging [63]. Thermal co-evaporation can overcome this reproducibility problem with its fine control over thin film deposition. Especially, for mixed halide perovskite cases, film quality can be improved via co-evaporation technique. Uniform thicknesses with smooth surfaces can be achieved as deposition rate is reduced for better film formation. Films without voids and pin holes are required for high efficiency devices to avoid shunting with transport layers [64].

Solution based fabrication with some configurations are chemically detailed and reproducibility can be problematic. To achieve high quality films by solution based spin coating, chemical addition to solvents prior to spin coating is the most common technique [65-73]. In these fabrication methods, precursors are dissolved in solvents such as dimethylformamide or y-butyrolactone before spin coating. Solvent complex then is removed by annealing [74]. Changing compositions of the precursors of MAX and PbX_2 is also studied widely [75-77] [51] [66-68]. Thermal co-evaporation can provide this film quality without further steps such as thermal annealing and additional chemicals. These additional steps are optimized in many investigations and observed their great influence the crystallization [75-81]. To use the advantage of fabrication simplicity of perovskite, these demanding techniques can be surpassed even though they are generally low temperature processes.

For large scale fabrication, vapor deposition techniques including thermal evaporation are superior over solution processes [82] [83]. One of the main goals of the future work is to achieve high efficient large area devices by thermal co-evaporation with mixed halide perovskites. The aim of this research can be refined as reaching the optical and structural conclusions from $MAPbI_{3-x}Br_x$ thin films with various Br/I ratio fabricated by using thermal co-evaporation technique of which deposition parameters are optimized.

CHAPTER 2.

EXPERIMENTAL METHODS

2.1 Frame of This Work

Characterization of perovskite thin films is one of the major ambiguities of perovskite research. The unstable nature of perovskite already makes the characterization steps susceptible to external effects. Different results of the same experiments are commonly encountered in the literature. Deposition technique, ambient conditions in which the sample is kept before the measurements, illumination status, measurement parameters and even the order of the characterization steps can change the results. Thus, researchers are not actually working on the same material unless these details are clear. The replication studies are valuable in that sense since they contribute to reach an agreement on the properties of perovskite and to move on further studies without questions.

Facile fabrication techniques along with excellent optical and electrical properties are tempting for researchers to get a deeper understanding about this promising material quickly. Solution process based techniques are appropriate and easy to reconfigure the parameters and engineer diversely. However, the unstable nature of perovskite, small grain sizes, surface coverage, uniformity and stoichiometry problems require more attention. Hybrid techniques depending on solution based fabrication still cannot resolve these problems although there are significant improvements. Structural and optical properties can be improved or comparable results can be obtained with solution based techniques with other techniques such as thermal evaporation.

Thermal evaporation technique studies demonstrate that perovskite formation by vapor in a fully vacuum environment is chemically feasible [82] [84]. In this method, the organic and inorganic constituent of perovskite is thermally evaporated simultaneously and reacts on the substrate to from the perovskite film. This method is called thermal co-evaporation because of this simultaneous evaporation of precursors. The basic difference from the solution based spin coating could be the compact and uniform film property since it does not depend on the wettability of the substrate surface. The co-evaporation deposition also allows controlling the film thickness more accurately. The morphology of the film can be optimized by the deposition parameters such as pressure and deposition rates with thermal co-evaporation. Moreover, homogenous film thickness and large scale void-free perovskite films are hard to achieve with the solution based techniques.

Intrinsic complexity of organometallic mixed halide perovskite hinders the use of characterization tools as in the case of other well-studied thin films. The instability problem of perovskite makes all conditions before and after measurement significant. UV-Vis spectroscopy, photoluminescence (PL), X-Ray diffraction (XRD) and scanning electron microscopy (SEM) were used by considering these remarks.

This thesis includes the band gap tuning of lead halide perovskite by mixing Br and I as halides. Br content in $CH_3NH_3I_{3-x}Br_x$ perovskite was increased by increasing the evaporation rate of Br including source material. Firstly, SEM and XRD measurements of the $CH_3NH_3PbI_3$ samples were done to optimize the fabrication parameters which are deposition pressure, deposition rate and annealing treatment with methanol. Five sets of deposition were done including two extreme points (0% and 100% Br content) with the parameters giving better crystallinity and morphology. Structural and optical characterizations were made simultaneously after each deposition. SEM and XRD measurements were used for structural analysis while UV-Vis and PL measurements were used for optical analysis.

2.2 General Details of the Experiments

All perovskite thin films were fabricated using Vaksis thermal evaporation system which has an evaporation chamber, a mechanical pump, a diffusion pump, power units, a CPU control unit and its PID controllers.

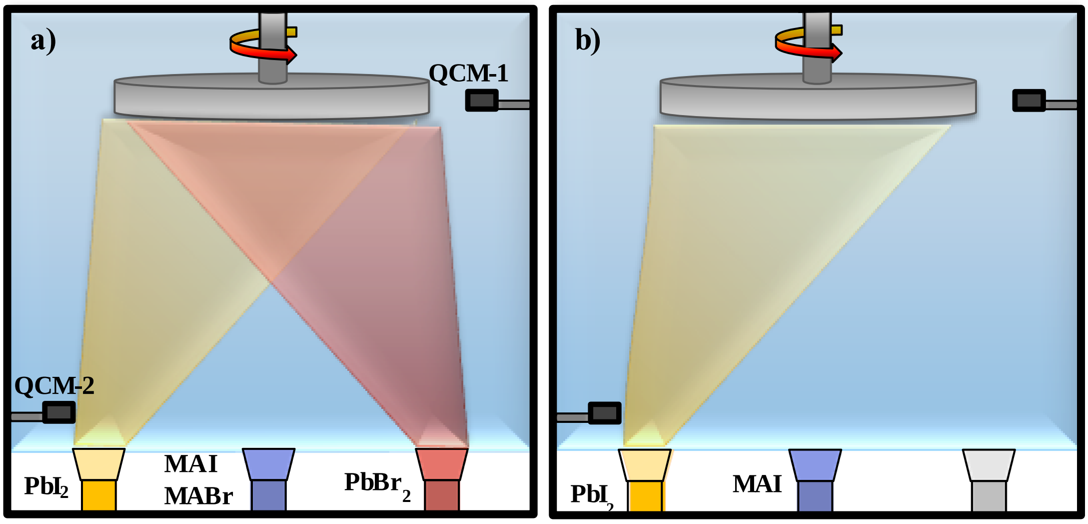

Figure 2.1: a) Three source deposition, b) two source deposition with the materials' name used in each cell.

For organic constituents, the source in the middle was used. MAI/MABr crucible was heated with a moderate power to avoid an unbalanced pressure and rate with sudden sublimation. Organic source shutters were closed during the whole deposition process as they filled the chamber as vapor unlike lead sources which hit the substrates more directionally. Organic source rate was controlled both by pressure and the total deposition rate which can be read at QCM-1 next to the substrate holder.

For MAI, QCM-1 starts reading the deposition when the temperature of MAI crucible reached to 150℃. The pressure rises when its temperature passed over 100℃ and as the temperature gets closer to 150℃, it reduces again. The cause of this pressure behavior is the release of humidity in synthesized MAI. Slow heating process helps MAI release its humid inside. After the temperature is increased over 150℃, both pressure and rate continue to rise. The pressure does not reach to the desired value when MAI temperature became above 185℃ the rate can be more useful for the deposition. The valve between the chamber and the diffusion pump was closed until the deposition pressure was reached to the desired value. For MABr, same pressure behavior with MAI was observed. MABr evaporation started at around 185℃.

The crucibles of the lead sources are heated simultaneously with MAI, but at a slower rate. When MAI reach its desired temperature to provide the deposition pressure, lead sources' temperatures are about 120℃. PbI_2 starts sublimating around 285℃ while $PbBr_2$ does it around 300℃. For the sample with no Br, PbI_2 was put in the crucible next to the QCM-2 in the Figure 2.1. The rate of PbI_2 was controlled by QCM-2 in this deposition. For the sample with no I, $PbBr_2$ was put in the third crucible which has no quartz sensor close to it. To control the rate of $PbBr_2$, total rate and MABr rate was checked regularly during the deposition. To get MABr rate, shutters of the $PbBr_2$ and substrate holder were closed briefly. For other depositions, PbI_2 and $PbBr_2$ powders were put in their own crucibles. Rate control was also done with the same procedures as explained. After starting sublimating, lead sources deposition rate increase linearly with the crucible temperature.

These temperatures may vary with the different systems as other works recorded different sublimation temperatures and rate-temperature relations [74]. For organic constituents, the air exposure time affects the evaporation temperature and pressure behavior. For lead halide constituents, the contamination amount of the crucible and the chamber walls affect the deposition behavior. The valve opening was changed accordingly to keep the deposition pressure constant. To keep the crucible contamination as a constant parameter and to keep the tooling factors of the QCM’s, the same materials are used in the crucibles in the same source.

In most of the studies reported in the literature, perovskite processes are performed inside nitrogen filled glove box. The presence of moisture influences the crystallization and re-crystallization of perovskite film whether it is fabricated in a dry ambient or not. To get a more realistic approach towards the future of perovskite, the degradation problems in air ambient processes must be resolved. In this work, the humidity was around 30% and the temperature was between 26-30℃ during the experiments. The humidity was quite low comparing the humid affected results in other studies and the temperature is well-below where any phase change or degradation happens [99]. The deposition process was in a fully vacuum ambient and the samples were kept in petri dishes covered with the plastic paraffin film, parafilm to avoid the humidity and aluminum foil to avoid photo-induced instability. No further caution was taken about instability issues and there was not any visible change occurred.

Perovskite thin films were prepared on VWR microscope slide pieces. The glasses were plain soda-lime glass constructed and cut into 2 x 2 cm pieces for the experiments. The substrates were cleaned by washing sequentially in Hallmanex detergent, acetone, and isopropyl alcohol by an ultrasonic bath for 10 minutes each. Then they were exposed to UV-ozone for 15 minutes just before the deposition.

The substrates were positioned on the holder with small claws by tightening the screws and transferred to the chamber. The weighted materials were put onto a plate where they crashed in to smaller pieces from their as processed crystal sizes. Then these powdery starting materials were put into the ceramic crucibles which were placed into the heating sources. After all the materials and substrates were placed vacuuming process starts. All the shutters were closed during the vacuuming process. First, the mechanical pump decrease the vacuum down to 1 x 10^{-1} Torr and the pre-heated diffusion pump starts. It took 2 hours to reach the base pressure 5 x 10^{-6} Torr on average. This base pressure was same for all the depositions in this work.

2.2.1 Material Synthesis

PbI_2 and $PbBr_2$ powders were purchased from Sigma-Aldrich and used as is. However, MAI and MABr powders were synthesized in the organic chemistry laboratory at the Department of Chemistry, METU. In the literature, different degrees of purity for MAI and MABr were reported. The purification removes the moisture inside the synthesized MAI/MABr. However, it is argued that some amount of the moisture was in fact needed for perovskite formation. Synthesis was done according to the well-documented and commonly-used recipe [85]. Both the MAI and MABr powder were synthesized by reacting 30 ml of methylamine (40% in methanol, TCI) and 32.3 ml of hydroiodic acid (57% in deionized water) or 23.3 ml of hydrobromic acid (48% in deionized water) in a 250 ml round bottom flask at 0℃ for 2 hours with stirring. The white subsidence was collected after removing the solvents carefully on a hot plate at 50℃ for 1 hour. The raw products were dissolved by stirring in absolute ethanol for 30 minutes. They were filtered and recrystallized in ethanol while being stirred. This washing process was repeated twice. The final products of MAI or MABr were dried at 60℃ in air. The synthesized materials were stored in small flasks, whose caps were wrapped with the parafilm and put in a desiccator when they were not used.

2.2.2 Optimization

Previous thermal co-evaporation studies demonstrated the details of the depositions and determined the possible parameters and conditions for better perovskite films. However, different setups and materials need the same optimization. For this purpose, deposition pressure and deposition rate with the post treatment of the samples were studied. Annealing is widely used to achieve better crystallization and stoichiometry. Annealing in methanol and humid ambient gives better results with the help of their contribution to the film. MAX compounds are soluble in water while PbX_2 compounds are not. Water’s being a partial solvent can be used to remove the excess MAX content from the film by thermal annealing in humid ambient. Other post-annealing studies also show that methanol improves the crystallinity [86] [87].

In this study, both humid and methanol annealing were performed for 10 minutes. During the annealing, 2 ml of methanol was added to 8 ml of water to get 20% methanol solution. The samples were subsequently dried in air on a hot plate for another 2 minutes.

To decide the deposition rate, only MAI and PbI_2 powders were used. The deposition rate was kept at 1.2 Å/s and 1.8 Å/s in total while the deposition pressure was 4 x10^{-5} torr. PbI_2 rate was kept 0.6 Å/s and 0.9 Å/s for these depositions accordingly.

Different deposition pressure values were also tried. The rate of PbI_2 and MAI is 0.6 Å/s each by the results of the rate study. Keeping the base pressure of the depositions at 5 x 10^{-6} Torr for all trials, four different deposition pressure, 3, 4, 5 and 6 x 10^{-5} torr were tested.

Film thickness was around 300 nm for all depositions which is a common value for perovskite devices [84] [88]. The deposition time was around 42 minutes with 1.2 Å/s deposition rate. The heating power of each cell, the chamber pressure, and QCM readings were followed constantly during deposition.

2.2.3 Band Gap Tuning Experiments

Band gap tuning by thermal evaporation depends on the chemical activity of the materials in vapor phase. Many experiments were done to understand how each constituent react in these pressure and temperatures. The QCM sensors were calibrated accordingly. The tooling factors and material densities were set before each deposition to control the exact rate. From previous results, the thicknesses of the films measured by SEM were used to fit the tooling factors of each sensor.

Two end points of bromide-iodide mixed perovskites were coated by two sources. The temperature and rates were decided by optimization study. To get $MAPbI_3$, MAI were heated up to 195℃ and PbI_2 were heated up to 285℃ with the rates of 0.5 Å/s and 0.3 Å/s respectively. To get $MAPbBr_3$, MABr were heated up to 230℃ and $PbBr_2$ were heated up to 320℃ with the same rates with MAI and PbI_2 respectively. This excess MAI and MABr rates were to keep the deposition pressure as desired and to keep the stoichiometry since the degradation affects the organic content first

[99]. Other source was left empty and heated up to 100℃ for degassing. To get the bromide-iodide mixed perovskites, PbI_2 and $PbBr_2$ were used for all three depositions. By changing their rates and the halide of the organic compound, band gap tuning was realized. Control of the three sources requires slower heating and slower changes as the total changes affect the pressure and the total rate synergistically. The temperature and rate details are explained in Table 2.1. $PbBr_2$ reached 0.4 Å/s rate at 325℃ and PbI_2 temperature was 280℃ for 0.2 Å/s rate. Bromide content of the perovskite thin films were decided beforehand as x equals to 0, 1, 1.33, 2 and 3 in the notation of $CH_3NH_3PbI_{3-x}Br_x$. The chemical reaction formulas of the depositions can be described by the following equations:

$$x=0: \quad CH_3NH_3I + PbI_2 \rightarrow CH_3NH_3PbI_3 \tag{2.1}$$

$$x=1: \quad \mathbf{2}CH_3NH_3I + PbI_2 + PbBr_2 \rightarrow CH_3NH_3PbI_2Br \tag{2.2}$$

$$x=1.33: \quad \mathbf{3}CH_3NH_3I + PbI_2 + \mathbf{2}PbBr_2 \rightarrow CH_3NH_3PbI_{1.67}Br_{1.33} \tag{2.3}$$

$$x=2: \quad \mathbf{2}CH_3NH_3Br + PbI_2 + PbBr_2 \rightarrow CH_3NH_3PbIBr_2 \tag{2.4}$$

$$x=3: \quad CH_3NH_3Br + PbBr_2 \rightarrow CH_3NH_3PbBr_3 \tag{2.5}$$

These values were the average values from the whole deposition duration. They were balanced at the desired points with the power and valve control. The starting materials were weighted and put into vials. The residues left in the crucible were minimized by calculating how much material was consumed for this thickness of films. Although fresh materials were used for each deposition, the expected rates were reached at different temperatures. These changes were not more than 10℃. The starting materials were prepared by crashing into smaller pieces caused these fluctuations. The diffusion pump valve was closed gradually until 3×10^{-5} Torr reached. The valve opening was reconfigured during the deposition to keep it steady.

Table 2.1: Deposition parameters of band gap tuning experiments

Dep.	Crucible 1			Crucible 2			Crucible 3			Diffusion valve opening
	Cont.	Temp (℃)	Rate (Å/s)	Cont.	Temp (℃)	Rate (Å/s)	Cont.	Temp (℃)	Rate (Å/s)	
x=0	-	-	-	MAI	195	0.5	PbI_2	285	0.3	24%
x=1	$PbBr_2$	325	0.3	MAI	200	0.6	PbI_2	285	0.3	20%
x=1.33	$PbBr_2$	335	0.4	MAI	190	0.6	PbI_2	280	0.2	16%
x=2	$PbBr_2$	320	0.3	MABr	230	0.6	PbI_2	285	0.3	16%
x=3	$PbBr_2$	320	0.3	MABr	230	0.5	-	-	-	30%

2.3 Characterization

Characterization of the semiconductor solids starts with the quantitative determination of properties such as carrier type, concentration, and mobility as electrically. For perovskites, these properties range in large scale and are influenced by the fabrication methods. Uniformity and smoothness of the samples are necessity for the characterization techniques which often consider the samples have a specific geometry [48]. Thermal co-evaporation method provides this uniformity and smoothness, but other intrinsic issues with the perovskite still remain.

As mentioned earlier, the measurements can be affected by pre-conditions. Thus, all the measurements were done right after the depositions and simultaneously. For each deposition, enough substrate was placed on the holder for all the measurements. All the samples are kept in air environment after the deposition. No illumination pretreatment was done prior to the measurements where perovskite properties can be altered in a controlled way [89].

The structural characterization of a thin film investigates the three dimensional arrangement of the atoms and molecules in solids. This investigation can cover the measurements of the lengths and the angles (the lattice parameters) inside the unit cell. In this work, the scope of structural analysis was only limited with X-ray diffraction (XRD) and scanning electron microscopy (SEM) which can reveal the crystalline state (single crystalline, polycrystalline, amorphous, etc.), surface and coverage quality of the deposition technique. Thermal co-evaporation technique needs further investigation starting from these basic methods.

The optical characterization of the samples was carried out by UV-Vis absorption spectrometry and photoluminescence (PL). The spontaneous radiative recombination inside the film results the light emission which is called luminescence. For many solids, the light emission is independent of the nature of the carrier excitation which can be from light, electricity, chemical reaction or applied voltage. For perovskite, the luminescence source is important since it can change the perovskite structure. The quality and quantity of luminescence also depend on the material. Photoluminescence which arises from the absorption of photons gives information about the material’s band gap. Since the emitted photons have equal or close to the energy of the band gap, PL measurements are useful for optical characterization.

2.3.1 Structural Characterization

2.3.1.1 SEM

Surface images of the perovskite samples are useful to observe the film morphology directly. SEM measurements give an opinion about grain size, coverage, uniformity and grain structure. In SEM technique, an electron beam is sent to the sample and scan across the surface. The scattered electrons are collected by detectors to form an image. Different types of detectors are present to collect all signals. There are different possible interactions with the beam and the sample to give various signals. Back-scattered, Auger, secondary electrons and cathodoluminescence with X-rays are generated [90]. The schematic of a standard SEM system is shown in Figure 2.2.

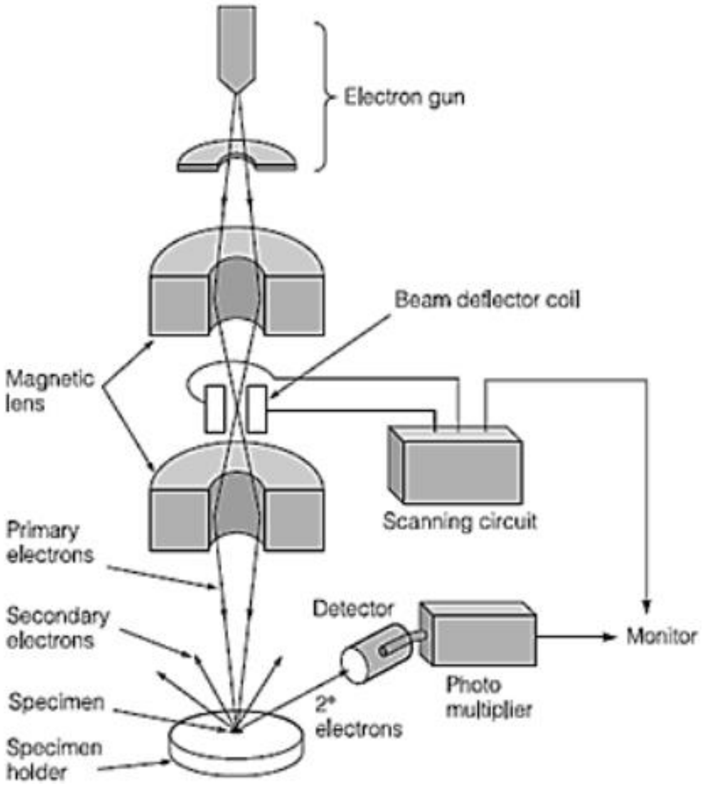

Figure 2.2: SEM equipment and the details of the process [91]

In this work, QUANTA 400F Field Emission model SEM equipment in the Central Laboratory of METU was used. The resolution of this device is 1.2 nm. The images were taken by two different magnifications for the mixed halide samples. One is for 1:100000 which has a scale bar of 1 μm and the other one is for 1:25000 which has a scale bar of 4 μm. Prior to analysis, the samples were coated with 10 nm gold-palladium to minimize the charging effect. Perovskite's intrinsic conductivity is not enough to avoid charge accumulation on the surface which causes damages on the surface and blurry images.

2.3.1.2 XRD

X-ray diffraction (XRD) is an effective tool to determine the atomic structure of crystalline materials. It is based on the principle of diffraction of electromagnetic waves in X-ray wavelength range which is shown in Figure 2.3.

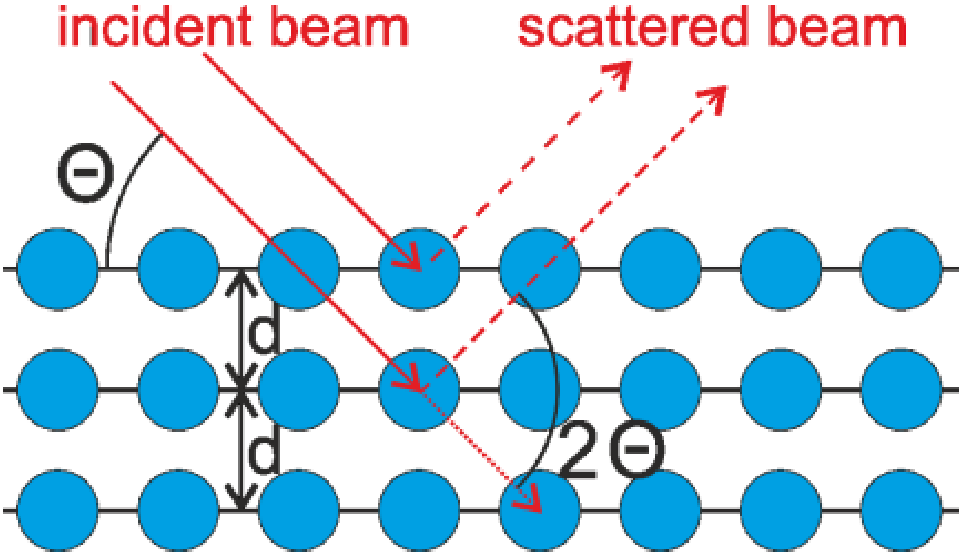

Figure 2.3: Schematic representation of XRD characterization principle [92]

Diffraction patterns are formed by the constructive interference from the periodic lattice structure. The process of X-ray diffraction in Figure 2.3 is followed by the Bragg's law:

$$n\lambda = 2d \sin(\theta) \tag{2.6}$$

where n is the order of the interference, λ is the wavelength of X-rays, d is the lattice spacing and θ is the angle of incidence [92]. In crystals, spherically spreading waves are formed by the scattered X-rays in different orders. The advantage of XRD is that it is non-destructive and an unknown crystal can be used without any information about it. To get the full insight about the crystallinity of a material, XRD is not enough. It should be supported by the element sensitive techniques such as XPS and EDS. However, XPS is only surface sensitive without sputtering and EDS is destructive to the perovskite film. EDX measurement for the samples with thicknesses used in this study also did not work as it receives signals from substrate which alter the result largely. The scope of this study was only limited to XRD for crystal information. To use XRD correctly, the angle between the planes and the incident and diffracted beams should be same, co-planar. The XRD spectrometers are calibrated in terms of 2θ which is the angle between the diffracted beam and the non-deflected beam. XRD peak positions and broadening size of the peaks provide adequate explanation to be used as evidence of homogeneous mixtures with high crystallinity. The asymmetric and broadened line profiles can be observed in XRD lines which are caused by the mechanical stress on the material or misplacing the sample in the measurement setup. To avoid the misinterpreted result, FWHM of the peaks was also calculated. FWHM is both a sign of instrumental broadening and the lattice scattering. Different type of XRD techniques are used in specific materials. In this work, powder method was used in which λ is fixed and θ is variable [93]. From this method, the shape and the size of the crystal can be deduced by the angular positions of the peaks. The data is then compared with the literature to compare our results.

Light exposure cause splitting the XRD peaks in a $CH_3NH_3PbI_{3-x}Br_x$ film, indicating that crystalline phases segregate with different Br containing perovskite sites [53]. For this, the measurements were held by loading the sample directly from the aluminum foil covered petri dish to the setup.

The XRD measurements in this study were conducted with Rigaku Miniflex X-Ray powder diffractometer in the Physics Department of METU. The schematic of the system is shown in the Figure 2.4. Cu K_α (0.154 nm) radiation was used as X-ray source. The scans were between 10° and 45° for survey measurements. The scan step was 0.05° and the acquisition time was 15 seconds per 1°. For (110) perovskite peak detection, the detailed scan was between 13.8° and 14.8°. The scan speed was decreased to 0.01° per one measurement and 300 seconds per 1°.

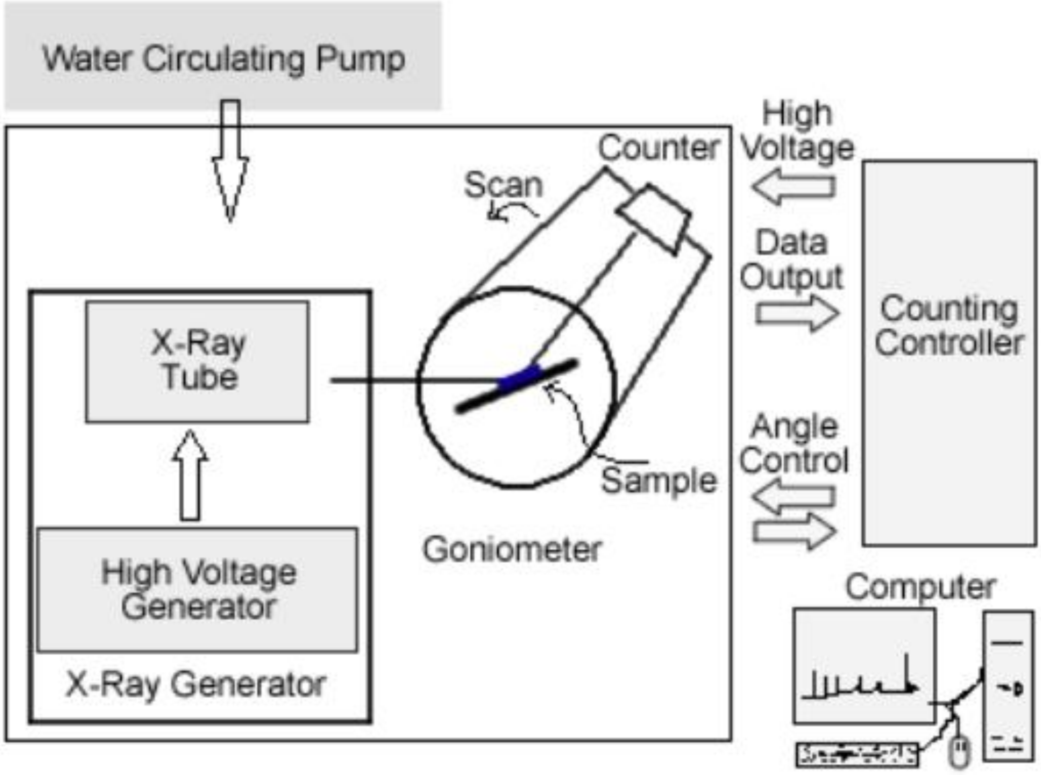

Figure 2.4: Schematic of the XRD setup [94]

2.3.2 Optical Characterization

2.3.2.1 UV-Vis Absorption Spectroscopy

The investigation of the band structure of a semiconductor with optical transmission or absorption spectrum is widely used. For semiconductors, incident photons with higher energies than the band gap energy excite an electron while the ones with lower energies are transmitted. Semiconductors with direct and indirect band gaps, however show different properties since this process is highly affected by the band gap type. The absorption coefficient of the samples was calculated by using the relation:

$$\alpha = \ln[(1-R(\lambda))/T(\lambda)]/d \qquad (2.7)$$

where α is the absorption coefficient, R and T are measured reflectance and transmittance data and d is the thickness of the sample. This formula measures the ratio of the number of the penetrating photons to the number of the penetrating photons which also pass through the sample. The unit of the absorption coefficient is cm^{-1}. The absorption coefficient was used to determine the optical band gap of the thin films. Tauc plot was used for this. The band gap of the material can be found by intersecting the plot with x-axis. The equation of this plot is given as:

$$\alpha h\nu = A(h\nu - E_g)^n \qquad (2.8)$$

where $h\nu$ is energy of the incident photon, E_g is band gap and A is a constant. The superscript n is dependent on the material type. For direct band gap materials, it is 0.5. To determine the band gap, the Tauc plot is linearly intersected to the x-axis from the optical band edge value.

Transmittance and reflectance measurements of thin films were done with UV-Vis spectrophotometer with an internally coupled integrating sphere. Only Si detector was used since the spectrum between 300 and 900 nm wavelength gives the desired information about perovskite band gap and optical behavior. The samples were constricted by the holders of the sphere in front of the circular slots.

2.3.2.2 Photoluminescence

For optoelectronic device applications, a non-destructive luminescence characterization for the fundamental optical properties is essential. Photoluminescence is a non-destructive technique and used either to detect the point effects or to measure the band gap of the materials. PL of a material basically includes excitation, thermalization and recombination processes. The excitation of a carrier can be between valance and conduction band as a hot carrier, between the band gap edges, from valance band to a trap state which generates an exciton, from a trap state to a level over conduction band edge or from conduction band edge to a higher energy level [95]. The recombination mechanisms vary with the material properties. Band-to-band, free-to-bound, donor-acceptor pair, excitonic and auger transitions occur between the electron-hole pair depending on the states they are at [96]. The recombination energy of the excited electron-hole pair will transform into non-radiative and/or radiative emission which is equal to the band gap energy for direct band gap semiconductors like perovskite. The produced photons can be specific to a defect site or characteristic to the material. To prevent this defect site effect contribution, different areas of the same samples were measured and the average of the measurements was taken.

The schematic of the PL setup is shown in Figure 2.5. Other than $CH_3NH_3PbBr_3$ (x=3) sample, all the samples were measured with the 532 nm green laser. For $CH_3NH_3PbBr_3$, UV laser with wavelength of 325 nm was used since the band gap of this sample was expected to be too close to the wavelength of the green laser. Laser beam was directed onto the samples via a path of various mirrors and passages preventing the stray light. The luminescent photons were collected by the Oriel model 77700a MS257 monochromator after focused by two lenses in front of the entrance slit. A notch filter was used to increase the signal to noise ratio and to cut-off the signal at the wavelength of the laser. The second grating of the monochromator was used which is 1200 lines/mm to resolve the obtained signal. This grating covers the visible and near infrared region. The grating selects the wavelength to transmit to the detector device. For light detection, the Hamamatsu C7041 multichannel detector which is a sensitive silicon charge coupled device

(CCD) camera was used. A LabVIEW program was responsible from the control of the monochromator by an RS232 port connection from the computer.

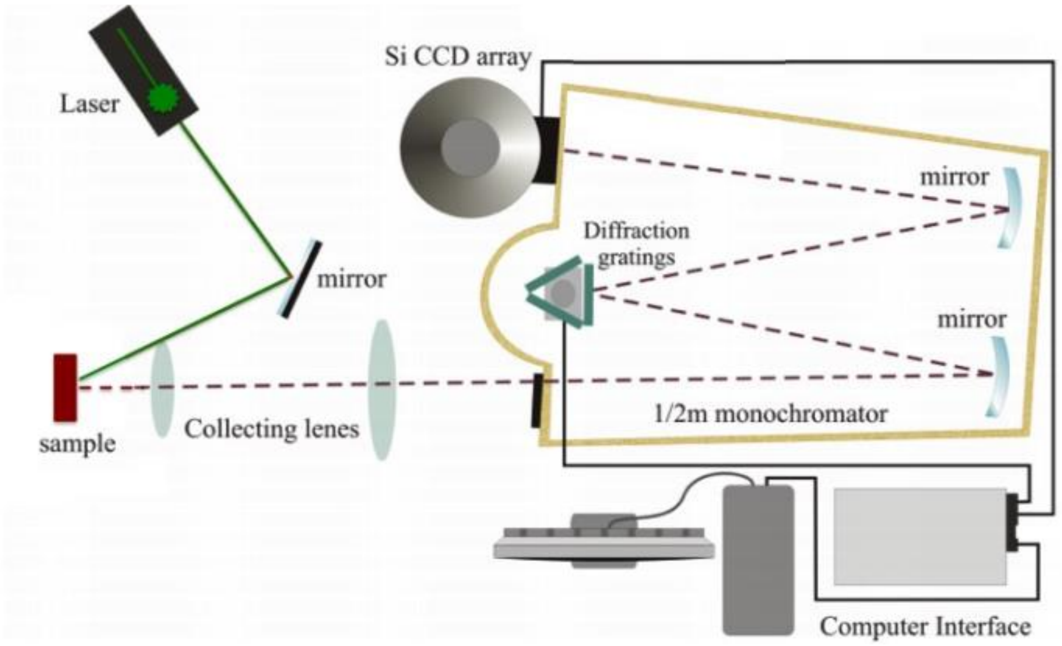

Figure 2.5: PL setup representation [95]

The power of the UV and green lasers are constant for all measurements. No power dependent luminescence intensity change was observed. However, the power optimization was done before the measurements with dummy perovskite samples since PL induced degradation was observed for high laser energies. The power of the laser was degrading the perovskite if it was exposed too long. The measurements were done at room temperature and to reduce the parasitic noise, all the other light sources in the dark room were turned off. Before each measurement, background noise was taken. Single shot measurement with hardware averaging of 500 was used.

CHAPTER 3.

RESULTS AND DISCUSSION

The basic motivation of this study is to tune the band gap of mixed halide perovskite by thermal co-evaporation method. We also aim at achieving compositional homogeneity of the thin films and compare with other techniques. The results are the representation of the combined study of a systematic research review and measurements of the optimized mixed halide perovskite samples which are still open to any further improvement and characterization. Optical and structural characterization results are correlated with each other. The thermal co-evaporation parameters were changed and their effects on the film properties are demonstrated. Absorption, band gap, grain size and crystallinity of bromide-iodide mixed lead perovskite thin films are discussed.

3.1 Optimization of the Deposition Parameters

SEM images of the $MAPbI_3$ thin films are shown in Figure 3.1. The deposition pressure of these samples was 4 x 10^{-5} torr. Large grains are marked with green lines on the images. The average grain size of the lower deposition rate samples are slightly larger than the ones with the higher rate. The average grain size for lower rate sample is ~200 nm and for the higher rate sample, it is ~150 nm. From the XRD peaks shown in Figure 3.2, it is clear that lower rate deposition have better crystallinity. XRD peaks of lower rate sample are more intense for each orientation. (110) and (220) orientation of crystals was observed for both cases. Lower rate sample also has smaller FWHM value which can be seen in Figure 3.2(b) for these peaks and therefore larger crystalline size. The diffraction peaks of the lower and higher rate samples are located at the same 2Θ values at 14.25°. 28.5°, 31.9°, 43.2° corresponding to the planes of (110), (220), (310) and (300).

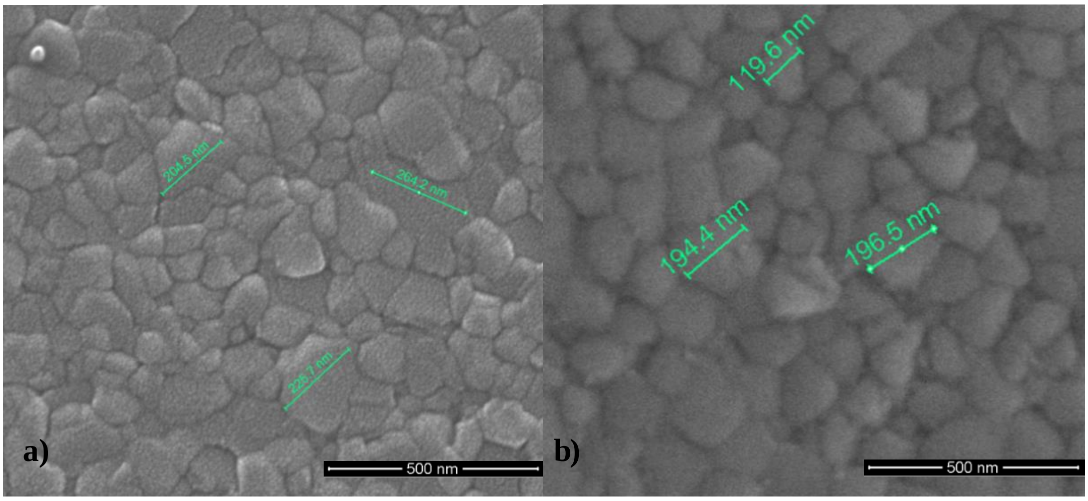

Figure 3.1: SEM images of the samples with MAI and PbI_2 rates of a) 0.6 Å/s, b) 0.9 Å/s.

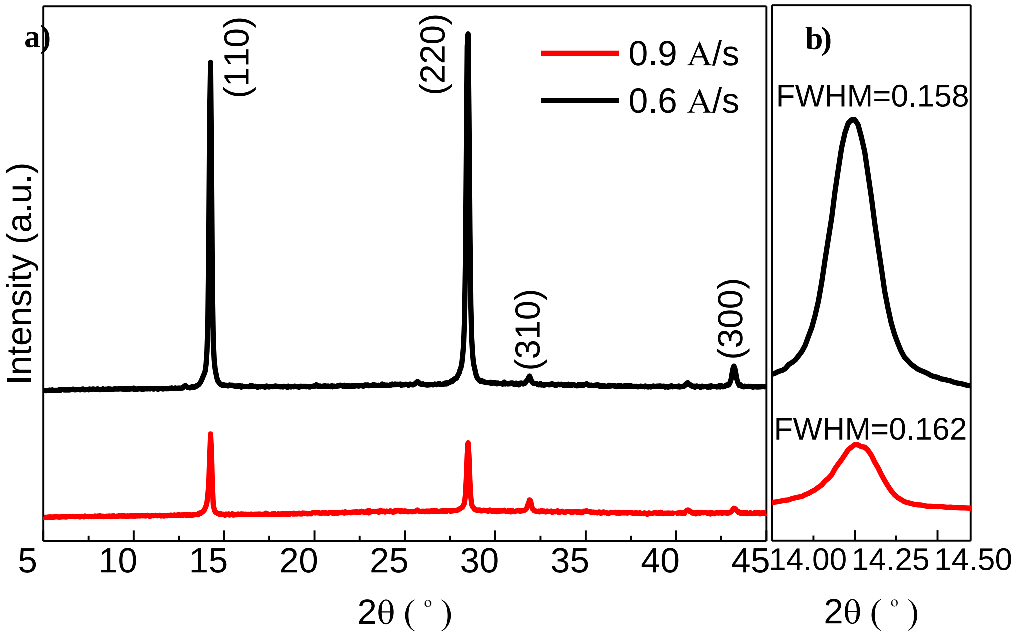

Figure 3.2: XRD results of deposition rate study. a) Survey scan between 5.0 and 45.0 degrees b) Detailed scan for (110) peaks between 14.0 and 14.5 degrees.

Lower rate was chosen for deposition pressure trials with 3, 4, 5 and 6 x 10^{-5} torr pressures. All the samples were first characterized before (as deposited) after annealing at 100℃ in methanol ambient for 10 minutes. Among these depositions, the samples which were fabricated at the deposition pressure of 3 x 10^{-5} Torr have the largest grain sizes which are shown in Figure 3.3.

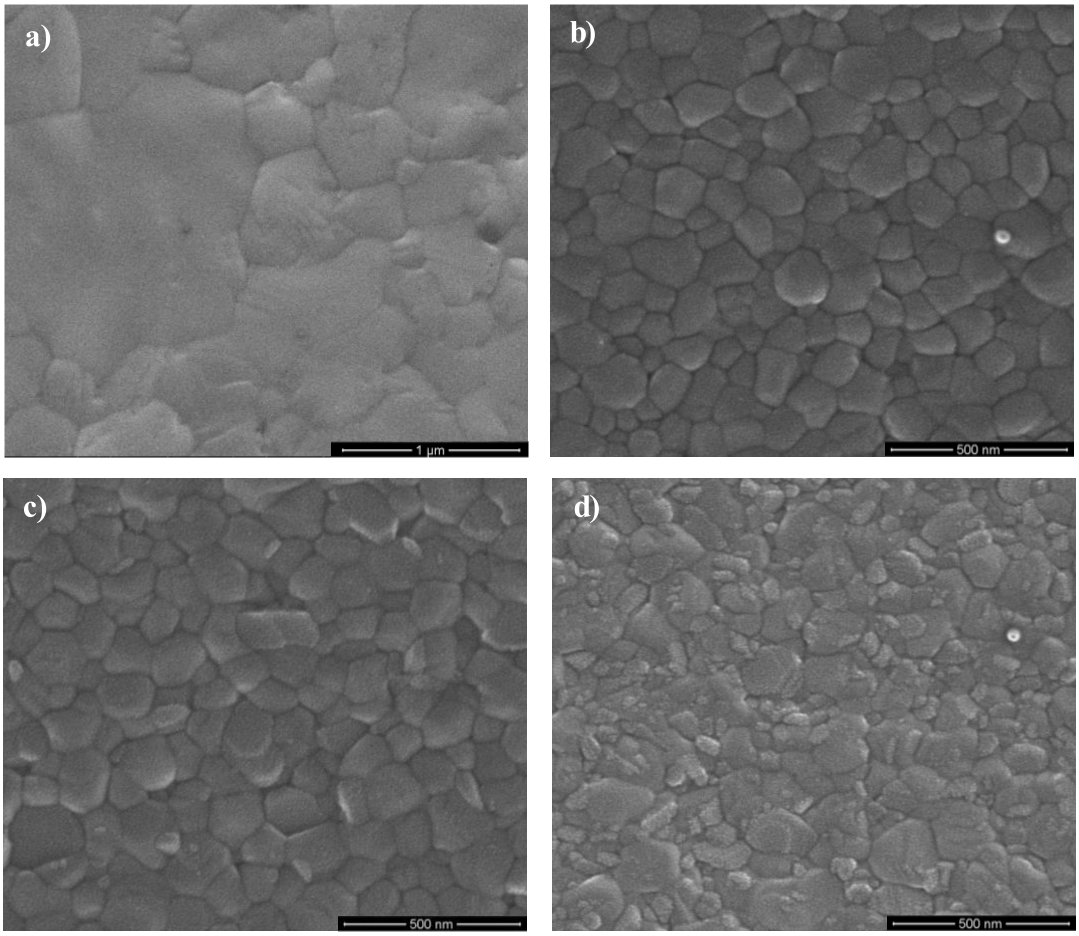

Figure 3.3: SEM images of the as deposited samples of a) 3 x 10^{-5} Torr, b) 4 x 10^{-5} Torr, c) 5 x 10^{-5} Torr d) 6 x 10^{-5} Torr

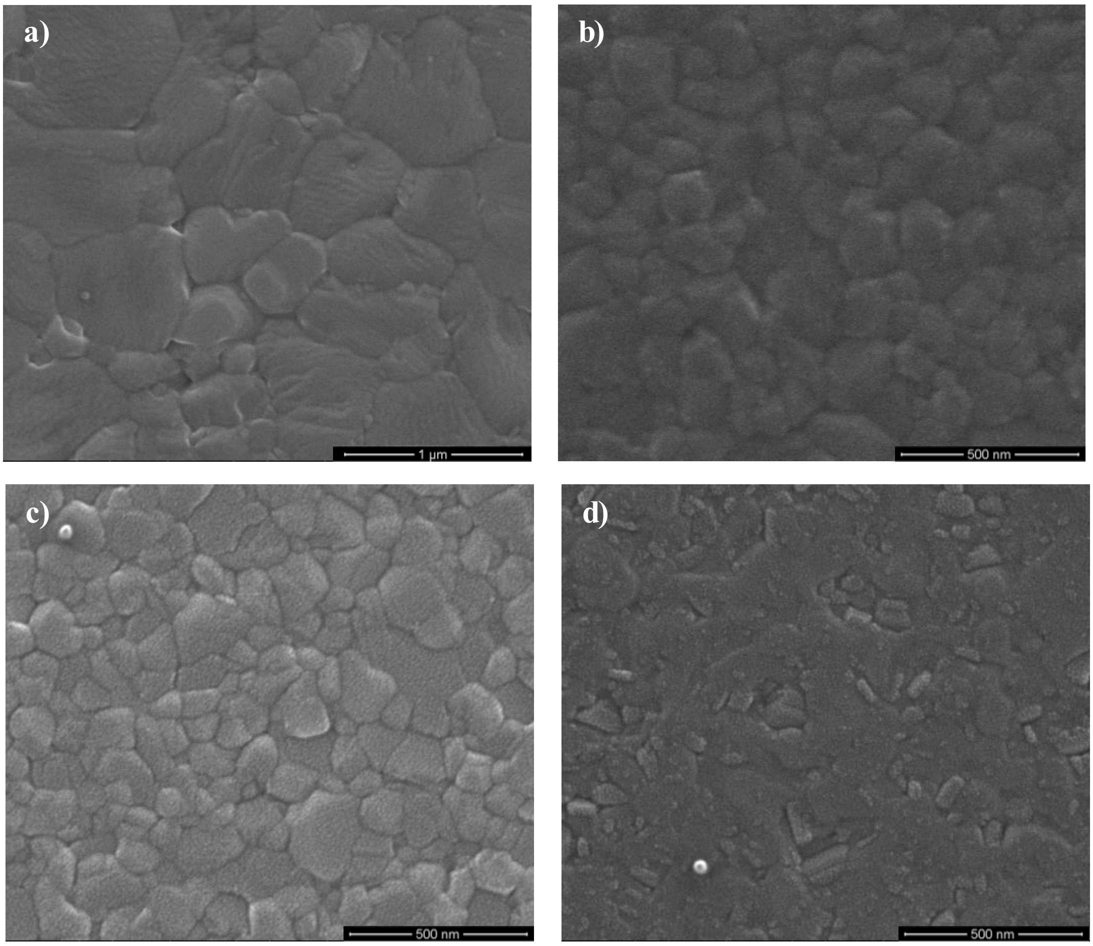

Figure 3.4: SEM images of the methanol annealed samples of a) 3×10^{-5} Torr, b) 4×10^{-5} Torr, c) 5×10^{-5} Torr, d) 6×10^{-5} Torr.

The grain size of 3×10^{-5} Torr sample is approximately ten times larger than samples deposited at higher pressures. Between the SEM images of all different pressure trials, both morphology and grain size has changed. Figure 3.3 and Figure 3.4 display that pressure control is a significant factor of deposition as the microstructure of the sample was totally changed. In these SEM images, other than 6×10^{-5} Torr, grain aggregation is not observed. All the grain boundaries are clear based on SEM images. For 6×10^{-5} Torr, the average grain size are smallest of all although there some larger grains between aggregated grains. For all the samples annealing treatment increase the grain size. However, for the sample with 3 x 10^{-5} Torr pressure, it does not make the same effect. Methanol annealing is a sensitive process. When the optimum methanol vapor amount is exceeded, the annealing process can result the otherwise. It is believed that this sample's situation was a result of poor conditioning of annealing step and needs replication for the further study. For the 6 x10^{-5} Torr sample, the annealing also caused some deformation. In this sample, grain boundaries became shaded and aggregation was observed.

The XRD results of the samples with different deposition pressure demonstrate that 3 x 10^{-5} Torr gives the best crystallinity among these values. Both peak intensities and FWHM values of the sample of this pressure are more satisfying than the others. From the survey scan in Figure 3.5, it is observed that (110) and (220) peak intensities are getting smaller with the increasing deposition pressure. FWHM values also indicate that crystalline quality of (110) orientation is getting better with the lower deposition pressure. (110) and (220) orientation are preferable for all depositions which seems typical for the depositions made in this system. The peak positions are 14.2°, 28.45°, 31.9° and 43.25° for the sample of 6 x 10^{-5} Torr while 14.35°, 28.6°, 32° and 43.3° for the sample of 3 x 10^{-5} Torr which correspond to (110), (220), (310) and (300) crystal orientation. The peak positions of the other two samples are between these values. These shifts are non-conclusive since they are very small however they show the same behavior for each orientation. There is a possibility of the misplacement of the sample to the device, but it is unlikely to cause a regular shift.

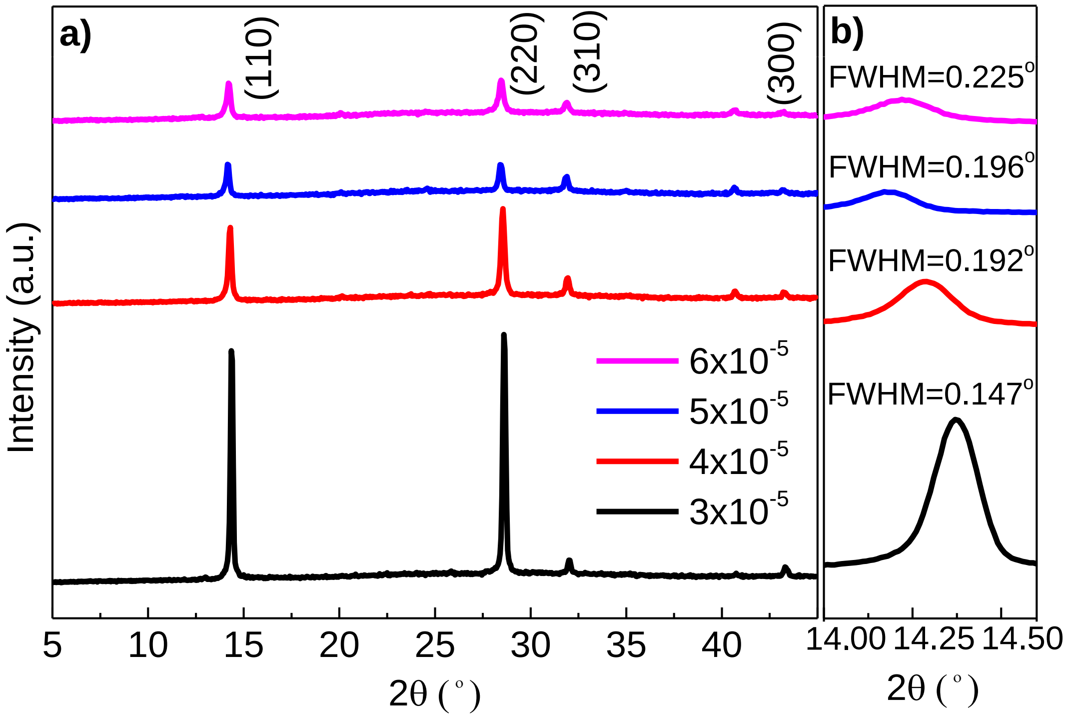

Figure 3.5: XRD lines of the as deposited samples of the deposition pressure study. a) Survey scan. b) Detailed scan for (110) peak.

The samples from the same deposition set were annealed in 20% methanol vapor ambient for 10 minutes at 100 ℃. The XRD lines in Figure 3.6 show the same trend with the as deposited measurements. Although SEM images indicate a clear grain size improvement, XRD peak intensities do not show the same observation. There are considerable increases in peak intensities, but they are not as high as expected when it is compared the improvement in grain sizes.

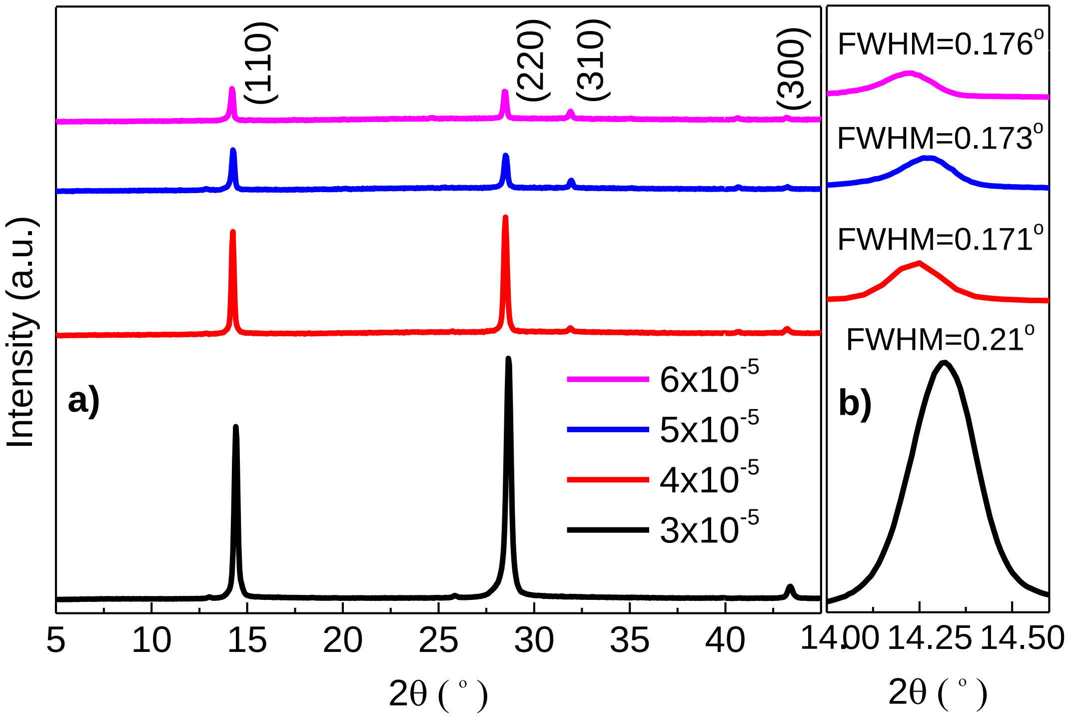

Figure 3.6: XRD lines of methanol annealed samples of the deposition pressure study. a) Survey scan. b) Detailed scan for (110) peak.

3.2 Structural Analysis Results

By the information obtained from the parameter study, mixed halide perovskite experiments were done with lower deposition rate which is 0.6 Å/s for each source and the lowest deposition pressure tested which is 3 x 10^{-5} Torr. Post treatment trial with methanol annealing needs further study to cover all the effects on perovskite formation and perovskite properties. The annealed samples are not conclusive with their SEM and XRD analysis. Methanol annealing process itself is very sensitive and also should be optimized in terms of annealing temperature and methanol concentration with the beakers used to generate vaporized ambient.

3.2.1 SEM Results

Figure 3.7 displays the SEM images of pure and mixed halide perovskite films. The morphology changes are also shown in Figure 3.8 with more detailed images. It is clear that the halide modification in mixed $MAPbI_{3-x}Br_x$ gradually alters the surface morphologies of perovskite films. All the films show perfect surface coverage which is a common issue with the spin coating technique [83]. Film uniformity with irregular boundaries are observed which is usual for poly-crystalline perovskites. The inclusion of bromide into perovskite leads to rougher surface morphology. The average grain size are decreased with the increasing bromide content. However, more detailed analysis is needed to make a certain conclusion. Other studies indicate that a phase transition occurs when x is over 0.2-0.4 for $CH_3NH_3Pb(I_{1-x}Br_x)_3$ mixed halide perovskites [32] [63] [97]. It can be observed in Figure 3.8 (b) that the largest grain size is obtained from x=1 sample. It is also depicted that bromide content has adverse effect after it crosses x=1. To be able to detect the exact x value that the grain size changes adversely, more experiments are needed.

The average grain sizes are very close to each other for x=1.33, x=2 and x=3 samples. The aggregation, on the other hand is increased with increasing bromide. The smallest grain size is obtained from the pure iodide sample. Grain size averaging is done by manually picking the grains with ImageJ software. There is no conclusive result about how Br content affects the crystal size in the literature yet. It depends on the fabrication technique, post-treatment conditions, phase purity, precursor mixtures and etc. The common feature for both pure halide and mixed halide perovskite surfaces is the granular and rather inhomogeneous topography. For the mixed halide thin films, there are different colored regions which points out different bromide contents of these regions.

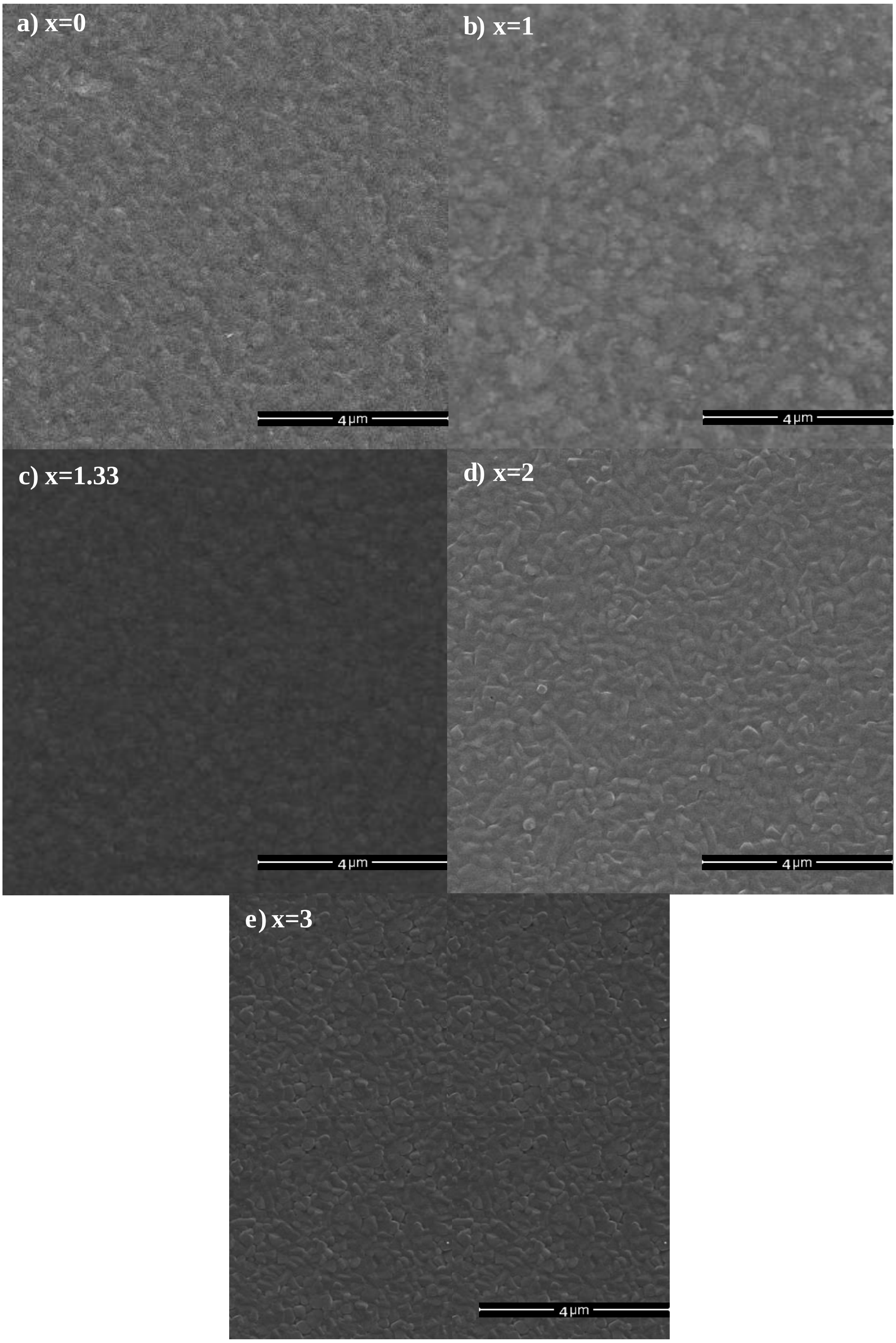

Figure 3.7: SEM images of mixed halide $CH_3NH_3PbI_{3-x}Br_x$ perovskites where a) x=0, b) x=1, c) x=1.33, d) x=2, e) x=3.

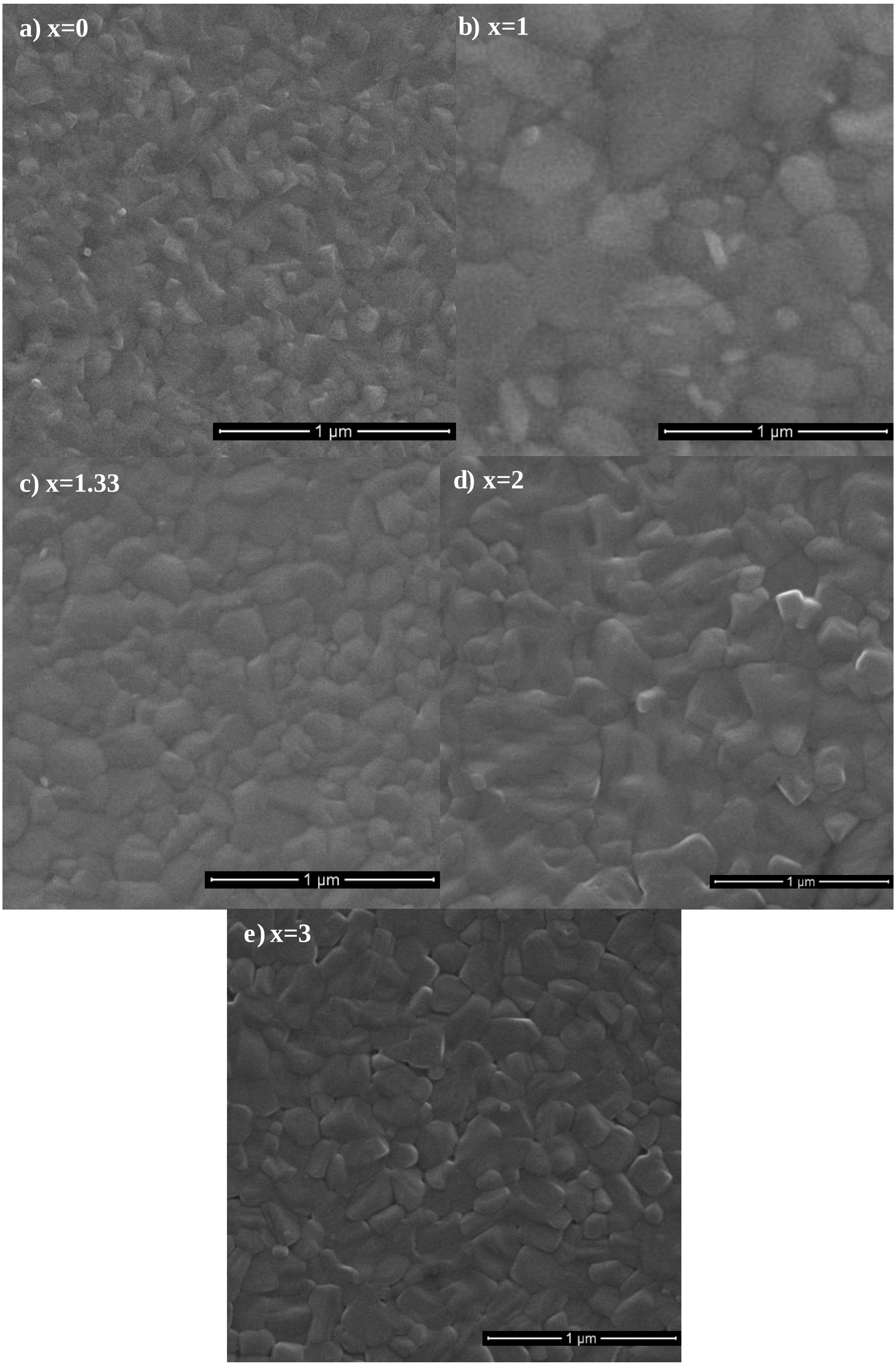

Figure 3.8: SEM images of mixed halide $CH_3NH_3PbI_{3-x}Br_x$ perovskites with 100000 magnification where a) x=0, b) x=1, c) x=1.33, d) x=2, e) x=3.

The measured samples were fabricated on VWR microscope slides. For each deposition, at least 8 pieces were present for simultaneous characterization. The sample sizes were 2.5 x 2.5 cm^2 as shown in Figure 3.9 and prepared for the characterization steps at clean room conditions.

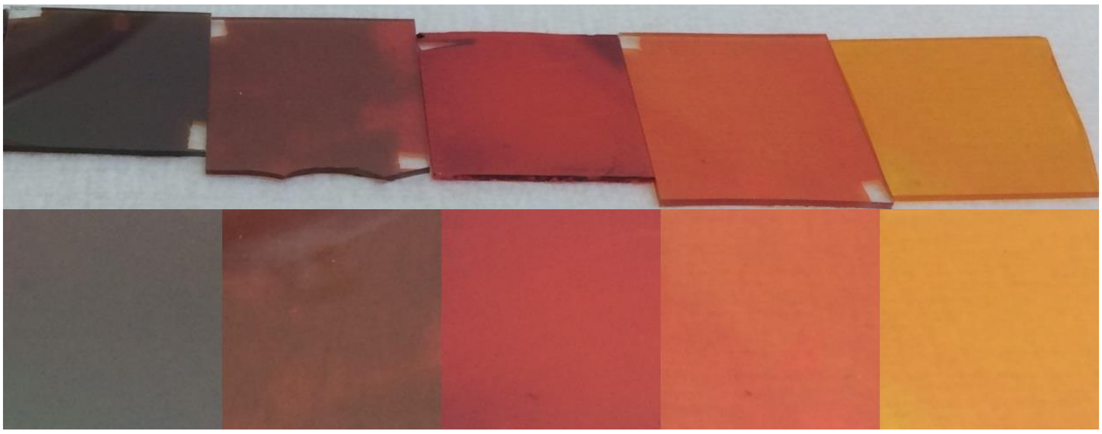

Figure 3.9: Photograph of the fabricated $CH_3NH_3PbI_{3-x}Br_x$ samples with increasing Br content from left (x=0) to right (x=3)

3.2.2 XRD Results

XRD patterns of these five perovskite films are depicted in Figure 3.10. All peak positions and expected shifts with bromide modification are in good agreement with the ones reported in the literature [32] [98-104]. As shown in Figure 3.10 with the survey scan, XRD peaks of $MAPbI_3$ are at 14.15°, 28.4°, 31.8° and 43.1° for (110), (220), (310) and (300) planes. It was shown earlier that (110) peak is in the tetragonal crystal structure [32] [105-107]. For $MAPbBr_3$, a cubic structure with diffraction peaks at 15°, 30.15°, 33.8° assigned as (100), (200) and (310) planes. The peaks of other three mixed halide samples are at the positions between these two extreme points. The diffraction peaks are at 14.45°, 29.05°, 32.5° for x=1 sample; 14.5°, 29.2°, 32.7° for x=1.33 sample; 14.75°, 29.7°, 33.3° for x=2 sample. The shifts are regular and follow the Br/I ratio change. The intensity of the peaks varies. Three samples ($CH_3NH_3PbI_3$, $CH_3NH_3PbI_2Br$, $CH_3NH_3PbBr_3$) result in better crystallinity in terms of crystal formation with narrow (110) or (100) peaks. Some traces of MAI and MABr with (200) orientation are also found in the x=3 and x=1.33 cases. In particular, (110) and (220) orientations of the crystalline $MAPbI_{3-x}Br_x$ are in favor. It is also observed in Figure 3.10 that (310) peak is increasing with the increasing Br content other than the sample $CH_3NH_3PbI_{1.67}Br_{1.33}$.

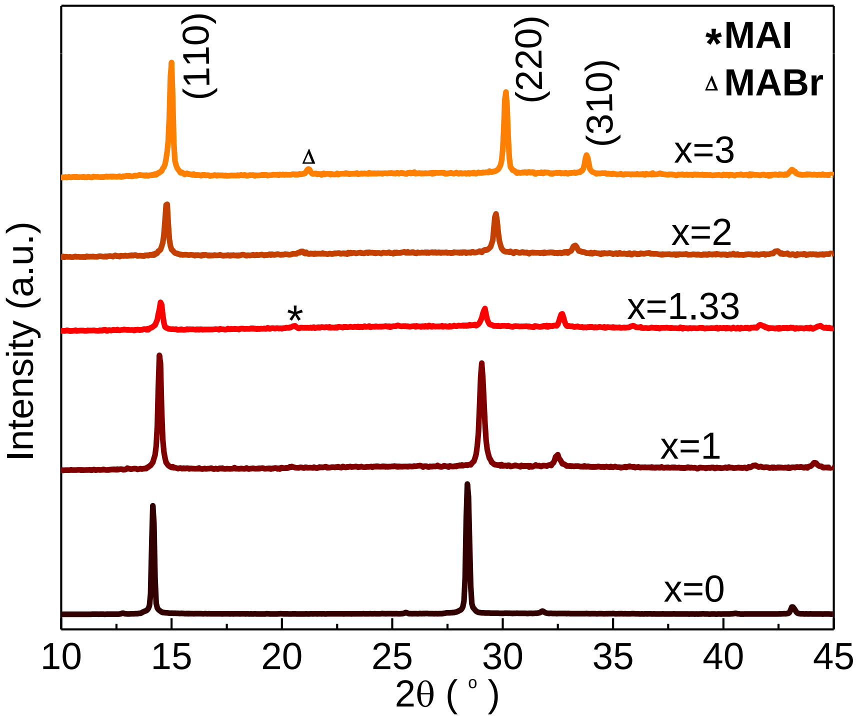

Figure 3.10: XRD lines of the perovskites with increasing Br content from bottom (x=0) to top (x=3)

The detailed scan of first perovskite peak is shown in Figure 3.11. The peak is shifting towards higher degrees gradually with increasing bromide. The orientation changes phase with this increase according to the previous studies [32]. The lattice constant increases with the increasing atomic size of the anions. There occurs this peak shift towards larger angles with the decreasing lattice parameter since atomic size of bromine is smaller than iodine.

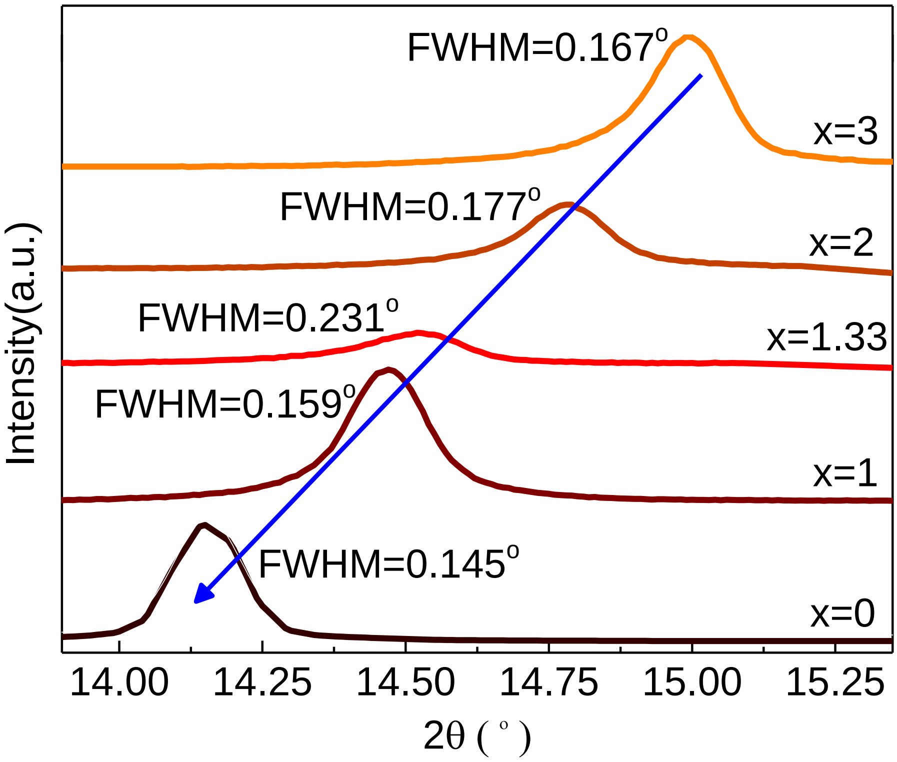

Figure 3.11: Detailed XRD scan of the (110) crystal orientation of the perovskite thin films with increasing Br content

By using Scherer formula shown in equation (3.1), the crystallite size in (110) orientation was calculated. The crystallite sizes are 29.53, 26.97, 18.57, 24.26 and 25.74 nm ordered by increasing Br.

$$D_p = (0.94 * \lambda) / (\beta_{FWHM} * \cos(\theta)) \quad (3.1)$$

where D_p is the crystallite size, λ (=0.1542 nm) is XRD radiation wavelength, β_{FWHM} is FWHM value and θ is the peak position in XRD plot.

Bromide-iodide mixed lead halide perovskite study is repeated many times to gain further insights about the intrinsic properties. One of these studies show how the diffraction peak range around 28°-30° with the bromide content in Figure 3.12. The analysis deepened with calculation of lattice constant to demonstrate the phase change observed in the crystal structure. It is also shown in Figure 3.13 that (110) peak positions and the shift is also similar.

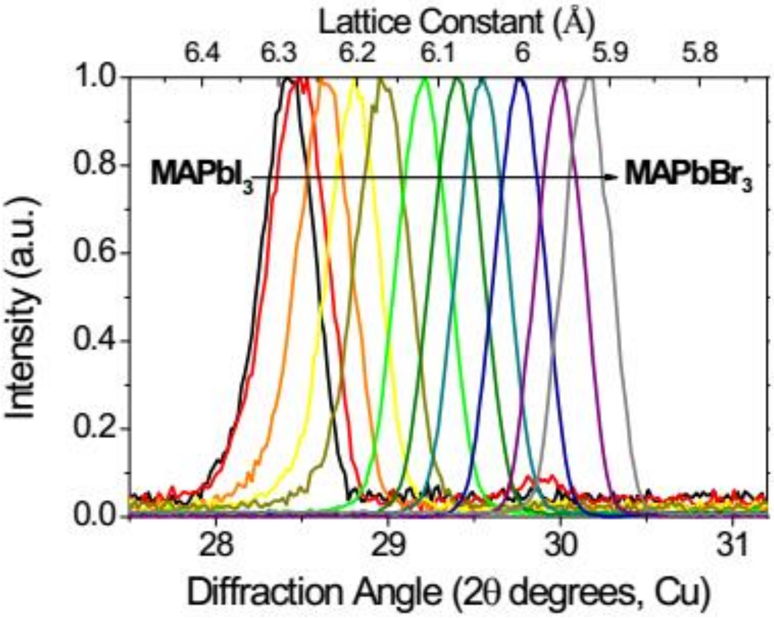

Figure 3.12: Normalized XRD patterns of mixed halide perovskite thin films showing the (220) (for $x \leq 0.1$) and (200) (for $x \geq 0.2$) diffraction peaks [51]

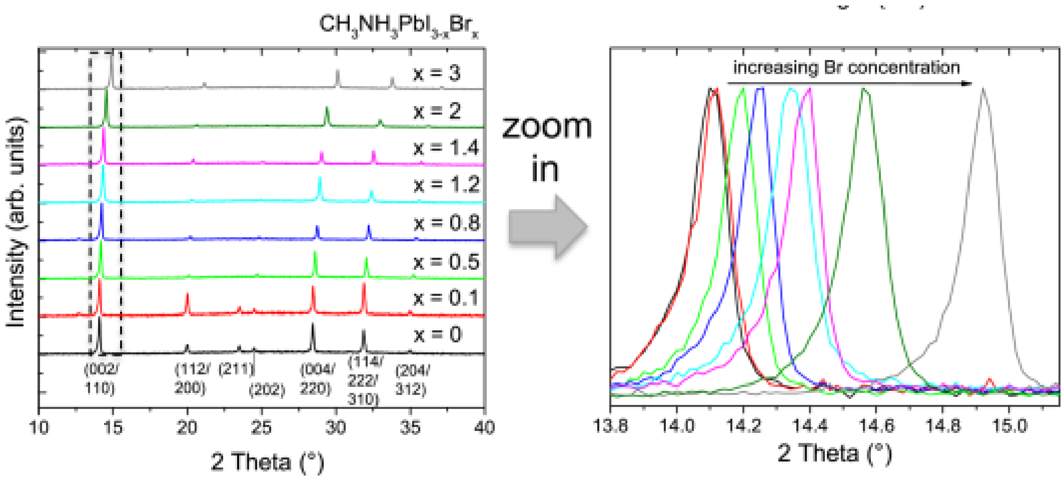

Figure 3.13: Gradual bromide inclusion to the perovskite structure on XRD patterns of [63]

3.3 Optical Analysis Results

UV-Vis absorption spectra and PL measurements were done carefully as they are destructive for perovskite samples. The incident time of the laser and light source can induce some physical changes which cause optical changes. Continuous PL measurement proves this assumption as it degrades the samples which can be visible by eye. Therefore, laser power was adjusted to get a whole measurement without causing any considerable change. The absorption measurement was done using an integrating sphere to collect both specular and diffuse transmission and reflection. This also prevents the effect of light scattering which is generated from refraction [51]. The optical band gaps are obtained from Tauc plots by using the calculated absorption coefficient which is explained in the experimental details section. Absorption onsets and PL peaks are also provided in Figure 3.17-21 and interpreted.

3.3.1 UV-Vis Absorption Spectroscopy Results

The absorption spectra of the mixed halide perovskite samples are shown in Figure 3.14. As the Br content increases, the absorbance edge shifts to shorter wavelengths. The absorption edges of the samples are not leveling off which indicates a clean band gap and sharp band edge. This clean gap is preserved as bromide content increase.

For pure bromide perovskite, $MAPbBr_3$, the absorption between 400 and 550 nm is higher than other perovskites which can indicate a better perovskite formation. In the same range, no other systematical change is observed with the bromide content difference. All of the samples have a good absorption in the visible range as a semiconductor. The shoulders formed in the mixed halide samples in the absorption plot denote sub-bandgap states which is caused by the increased disorder in the films.

The absorption onset of $CH_3NH_3PbI_{3-x}Br_x$ changed systematically from 810 nm to 580 nm with increasing bromide fraction, consistent with observations in recent studies [32] [70] [108]. Pure iodide lead halide perovskite bulk crystalline was also reported to have an absorption onset of about 820 nm [109]. The onset values are 1.53, 1.67, 1.73, 1.88 and 2.14 eV in energy unit at which x values are 0, 1, 1.33, 2 and 3.

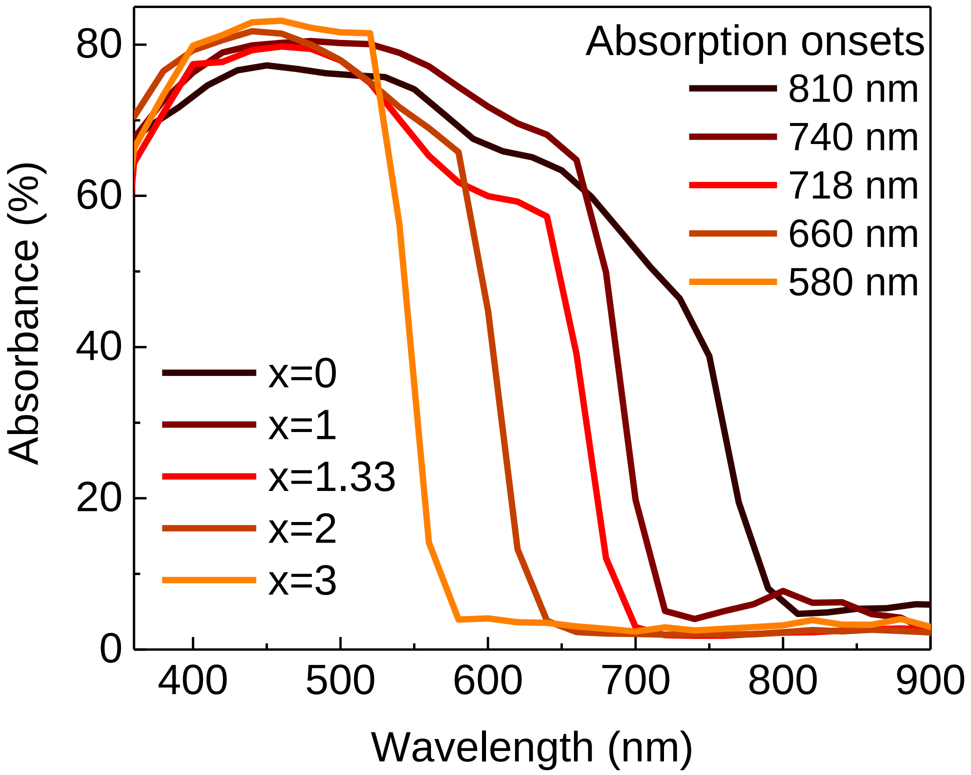

Figure 3.14: Absorption spectrum of the samples with absorption onset values

The optical band gaps were extracted from Tauc plots, shown in Figure 3.15. The values found here are almost exactly the same as the values found by Noh et al [32]. Linear fit of the Tauc plot is clear for each sample, meaning also a sharp band states. Except for x=1 sample, all the optical band gap values are higher than absorption onset values. The differences are as low as 0.1 eV which is desired for thin film absorbers [51].

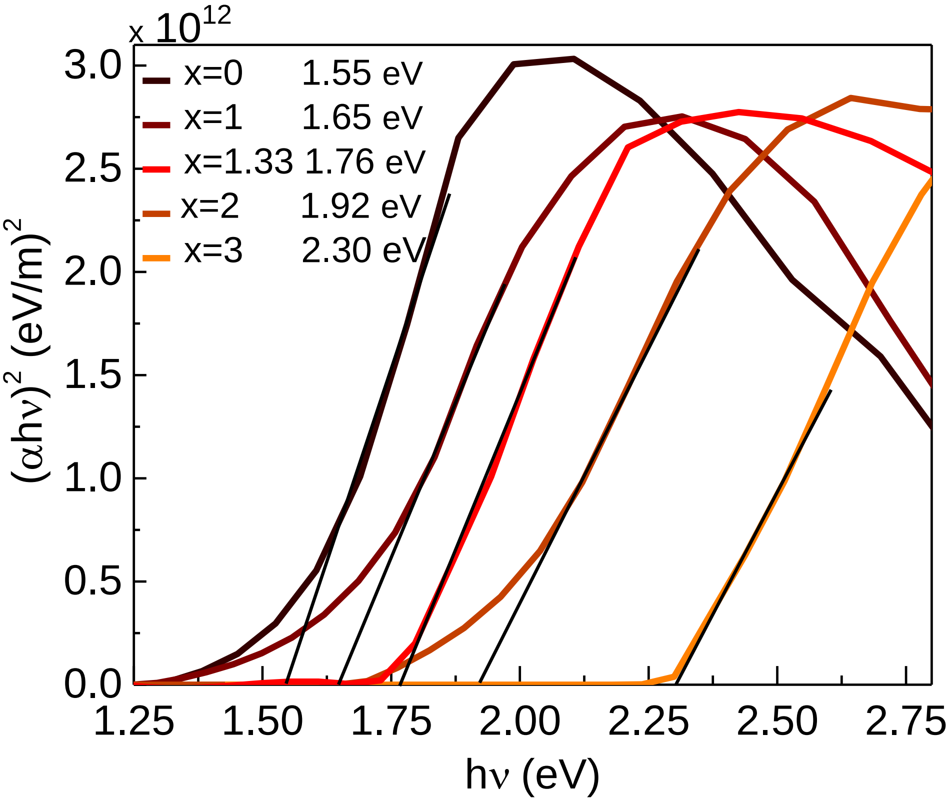

Figure 3.15: Tauc plot of $CH_3NH_3PbI_xBr_{3-x}$ samples with varying I/Br concentrations

The band gap and bromide content relation is shown in Figure 3.16. The previous studies suggest that empirical fitting of band gap values and bromide content can give an opinion about other non-tested values and fluctuation degree in the crystal field [114]. The non-linear fitting shows the anisotropic nature of binding [110]. The non-linear fitting has different constants for different studies [32] [63] [97] [111]. By using the equation (3.2), one can find a parameter about compositional disorder.

$$E_g(x) = E_g(MAPbI_3) + [E_g(MAPbBr_3) - E_g(MAPbI_3) - b]*x/3 + b*(x/3)^2 \qquad (3.2)$$

where b is the bowing parameter reflecting this anisotropic nature of binding [110] [112] [113]. From the fitting constants applied to the equation, the value of b from this relation is found 0.53 eV. This moderate value of b shows that there is compositional disorder at some degree. The linear fit does not give a conclusive result. The existence of impurities and crystal disorders discredit the linear fit which was used in another study with similar band gap values but different absorbance [88].

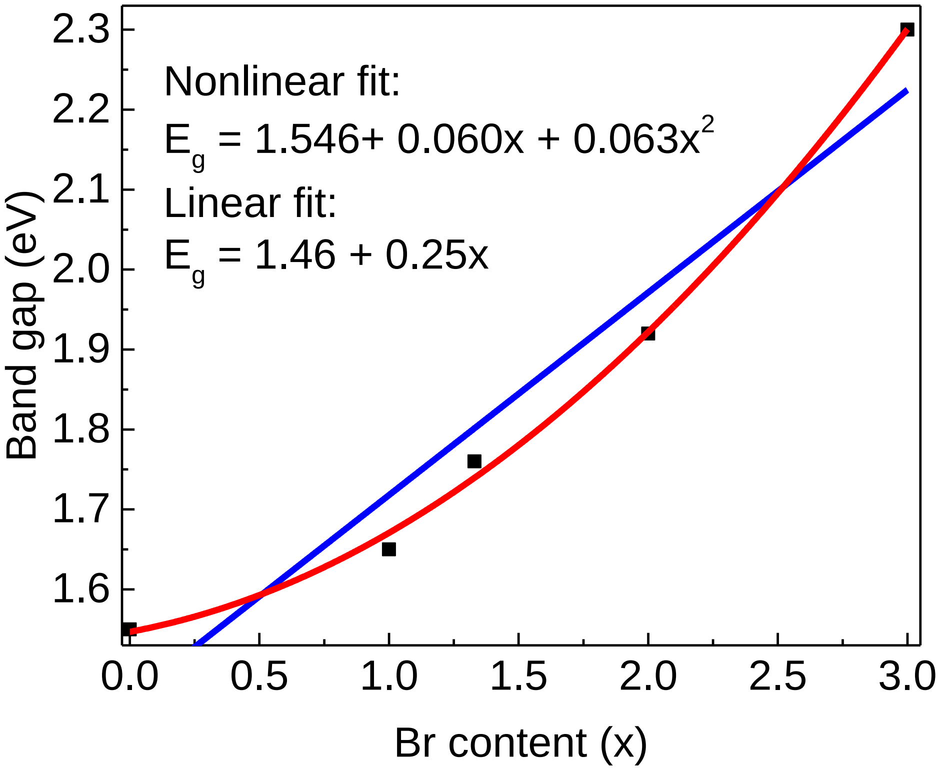

Figure 3.16: Optical band gap with empirical Br contents of $CH_3NH_3I_{3-x}Br_x$ perovskites and the linear and quadratic fitting for the band gap-Br content relation

3.3.2 PL Results

The laser power has a great importance in measuring PL since low intensities can result in trapping of photo-generated charges as much as radiative recombination which means reduced luminescence [114-117]. This power sensitivity is also affected by bromide content. Bromide rich perovskites are more prone to the changes by the overpower [63]. When the excitation increase with the sufficient laser intensity, the trap states are filled first and luminescence can dominate. In this study, power of the laser is adjusted to a non-degrading value while being sure that enough luminescence created.

PL measurement data and the absorption spectrum are plotted in the same figure for each sample to compare the absorption onset value and PL peak position in Figure 17-21. The values for the $CH_3NH_3I_{3-x}Br_x$ samples with x=2 and x=3 are not matching. The matching values indicate that absorption and emission originate from similar states. For x=2, it is red-shifted while the PL peak is blue-shifted for x=3.

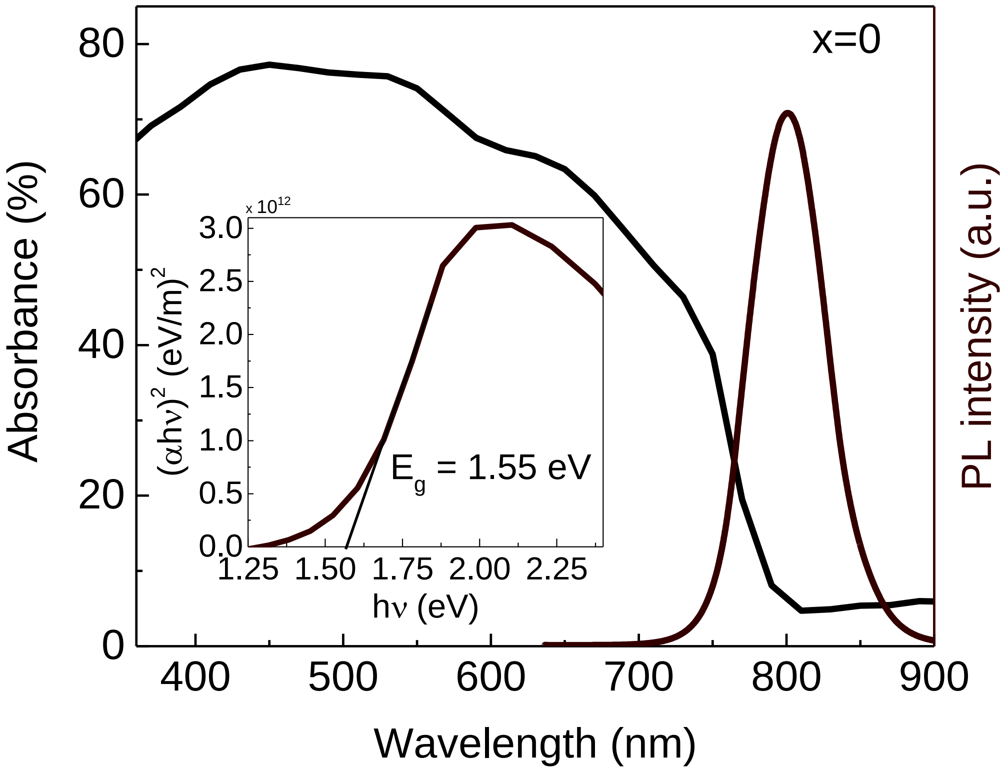

Figure 3.17: The absorption plot with PL peak of $CH_3NH_3PbI_3$ sample. The inset is Tauc plot of the same sample.

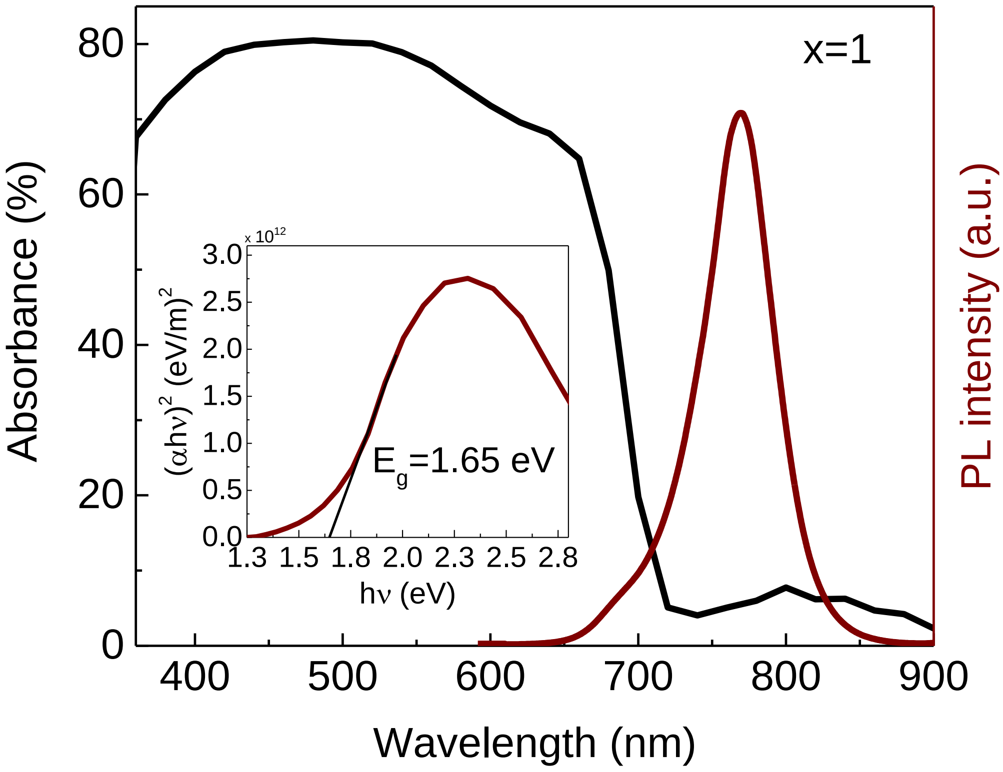

Figure 3.18: The absorption plot with PL peak of $CH_3NH_3PbI_2Br$ sample. The inset is Tauc plot of the same sample.

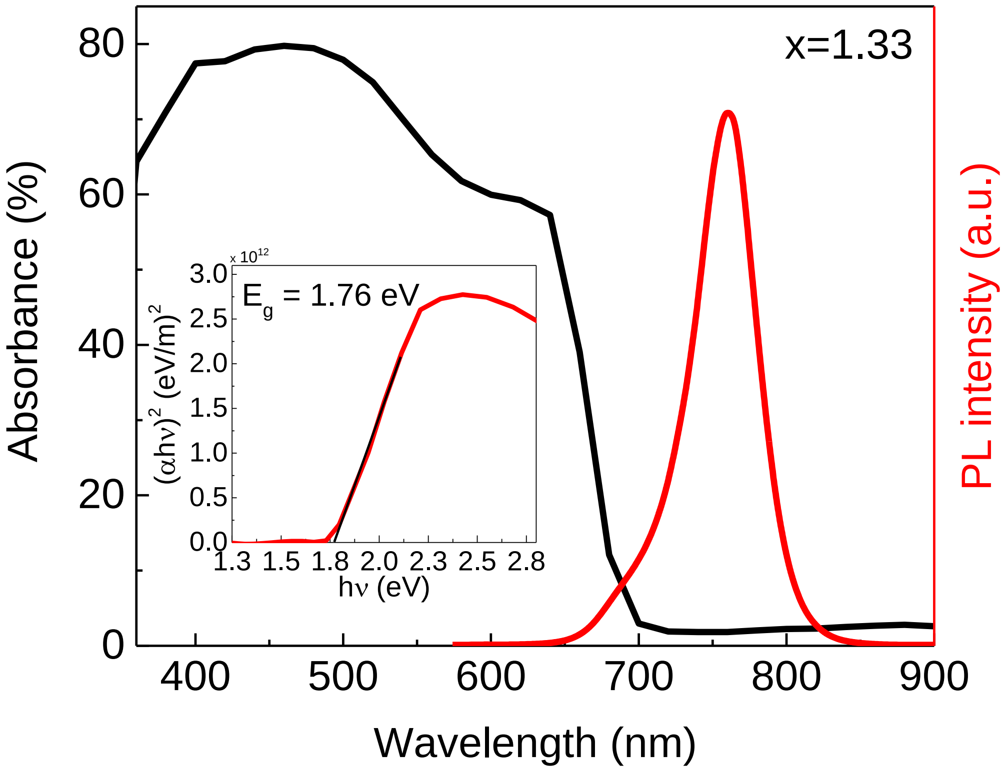

Figure 3.19: The absorption plot with PL peak of $CH_3NH_3PbI_{1.67}Br_{1.33}$ sample. The inset is Tauc plot of the same sample.

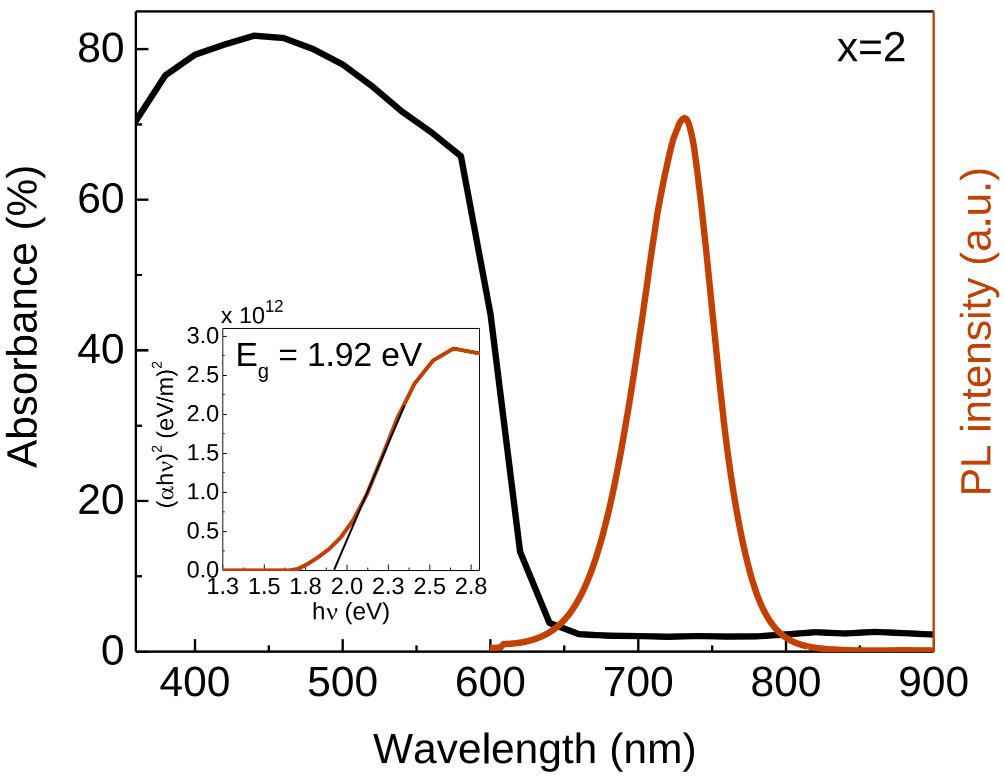

Figure 3.20: The absorption plot with PL peak of $CH_3NH_3PbIBr_2$ sample. The inset is Tauc plot of the same sample.

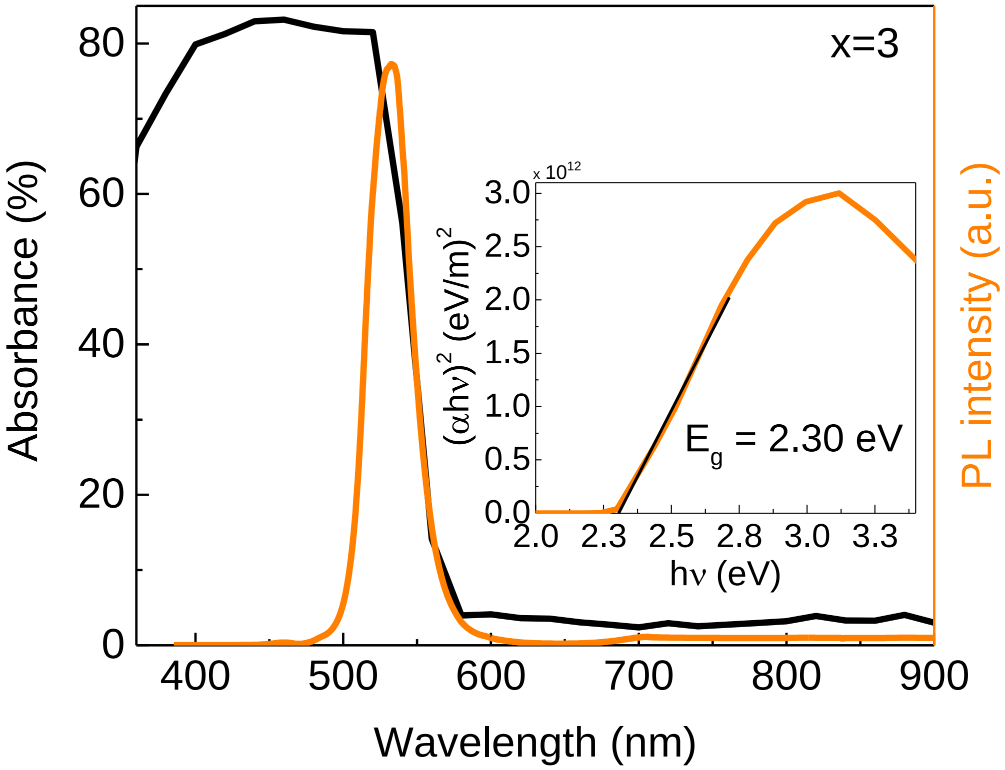

Figure 3.21: The absorption plot with PL peak of $CH_3NH_3PbBr_3$ sample. The inset is Tauc plot of the same sample.

PL patterns shown in Figure 3.22 are normalized to observe the shift of the emission peak clearly. The peak positions follow a similar trend with iodide fraction which supports the finding that gradual Br substitution by thermal evaporation is a straightforward process by increasing Br evaporation. The peak shift also indicates that the recombination centers are generated in the lattice structure with bromide and iodide co-presence. The shift is also consistent with the previous studies [97] [118] [119]. The absorption onsets are 580, 660, 718, 740 and 810 nm in order of decreasing bromide. For the mixed halide perovskites, there is a clear red-shift in the PL peaks which can be a result of halide migration, meaning of iodide-rich domains [51].

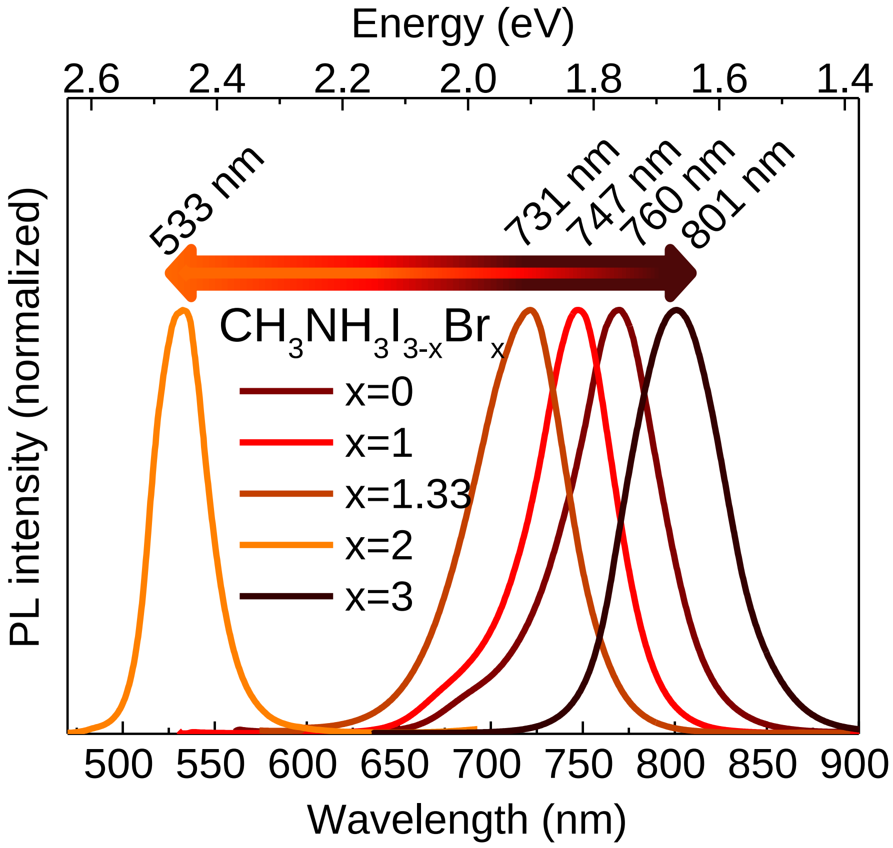

Figure 3.22: Normalized PL peaks of the $CH_3NH_3I_{3-x}Br_3$ samples

For intermediate contribution of bromide to the perovskite structure, the PL energy of the sample which is around 1.67-1.68 eV remains invariant [120]. This finding support the Stokes shift in the mixed halide films in this study. It means that luminescence is generated at the deep levels in the band gap. Halide migration and lattice relaxation are the possible reasons of Stokes shift shown in Figure 3.23 [97].

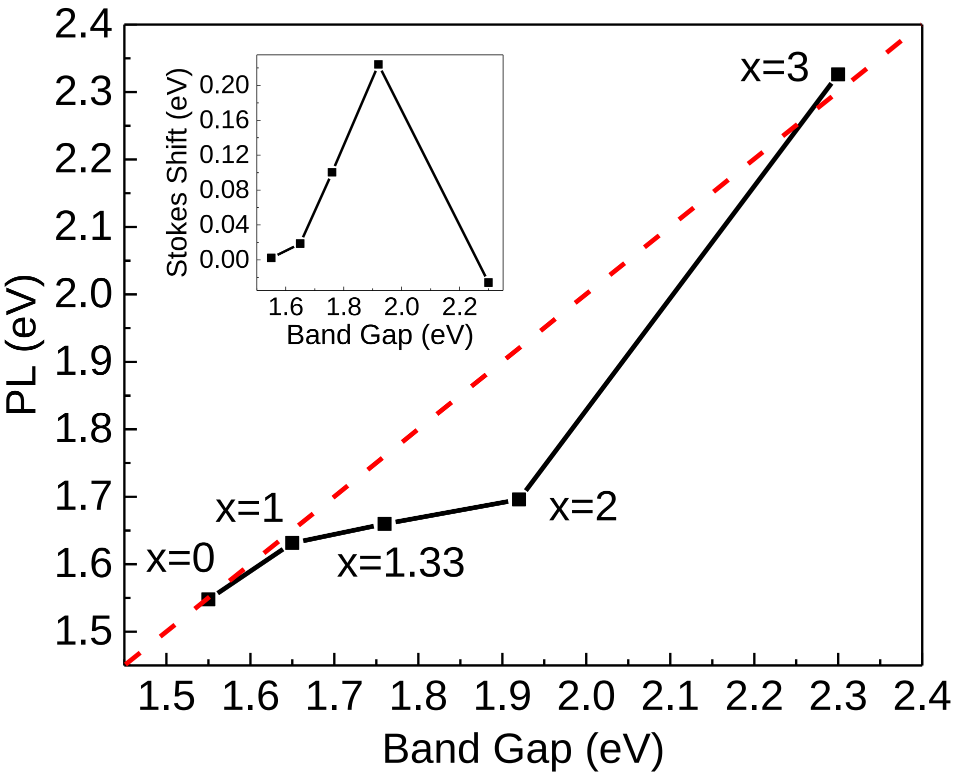

Figure 3.23: PL peak and optical band gap comparison to determine the Stokes shift

The optical band gap determination of perovskite films from PL data is tricky because of all the susceptible details of both measurement and physical concept of perovskite. PL in mixed and pure perovskite can be observed in the same samples if there is phase segregation in the film. Low and high energy tails of the PL peak cause an asymmetric PL pattern. By deconvoluting the PL pattern using Voigt formula for fitting shown in Figure 24-28, this tail states can be found. From the fitting quality, it can also be deduced the single phase status of the sample. Other than x=2 sample, original PL peak and the higher valued deconvoluted peak have almost the same position as all the fittings are well-matched with the original data.

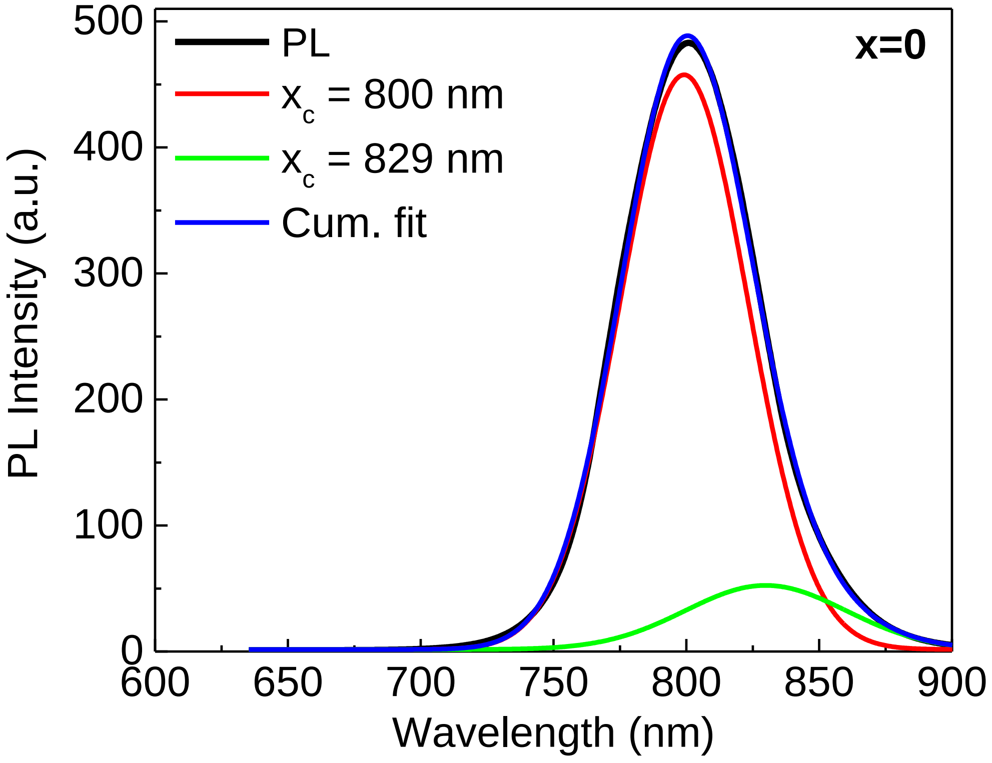

Figure 3.24: PL deconvolution of the pure iodide perovskite sample

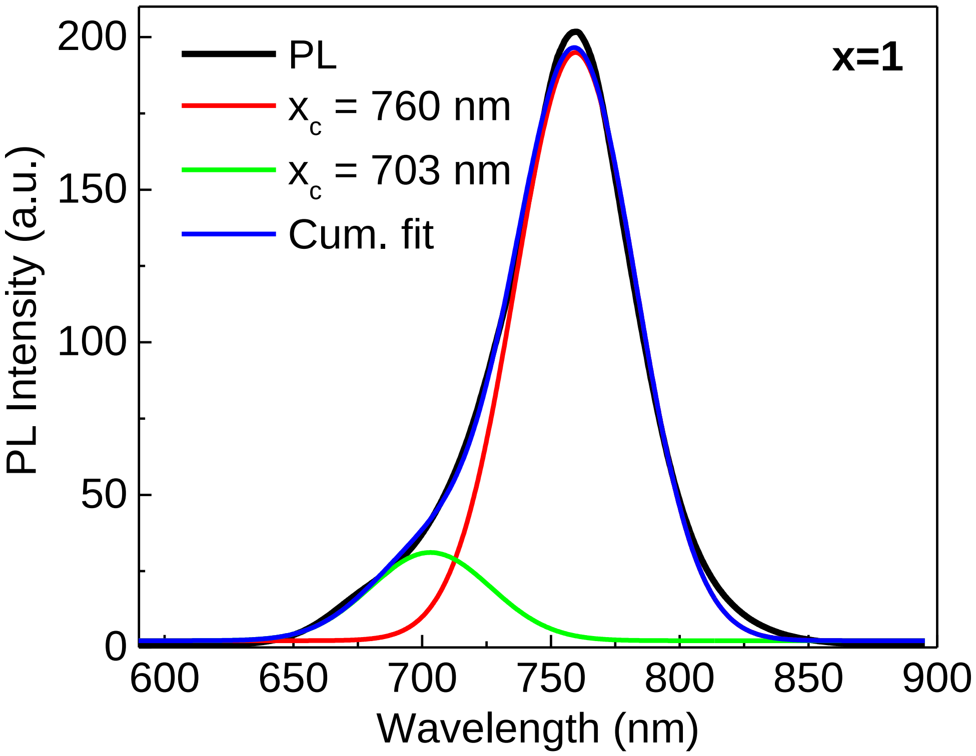

Figure 3.25: PL deconvolution of the $CH_3NH_3PbI_2Br$ perovskite sample

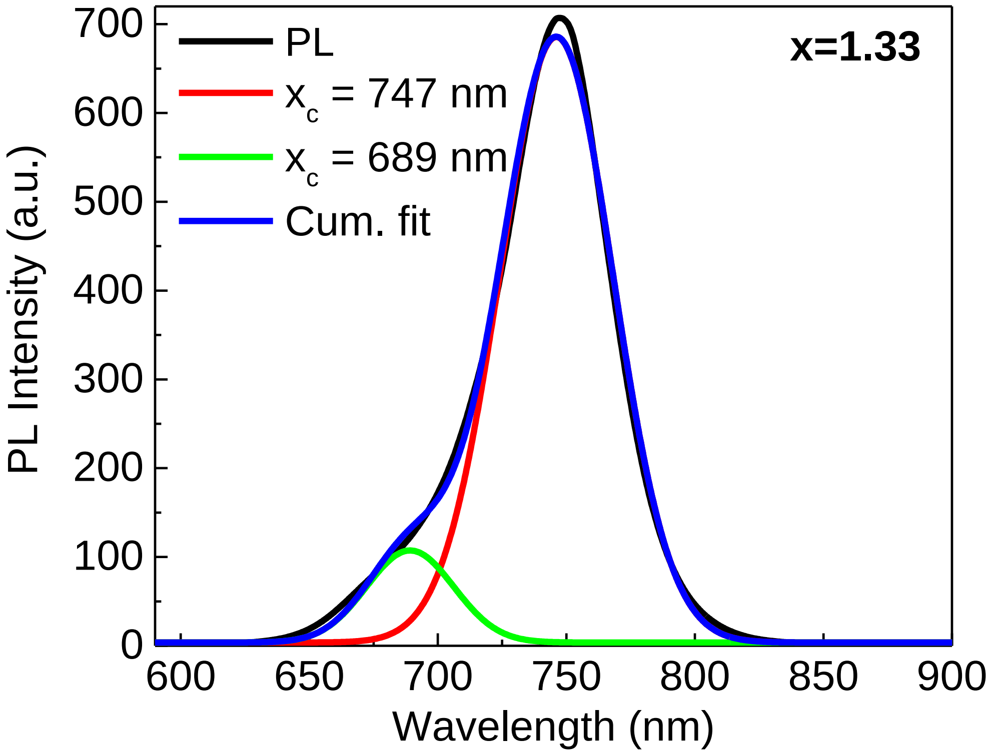

Figure 3.26: PL deconvolution of the $CH_3NH_3PbI_{1.67}Br_{1.33}$ perovskite sample

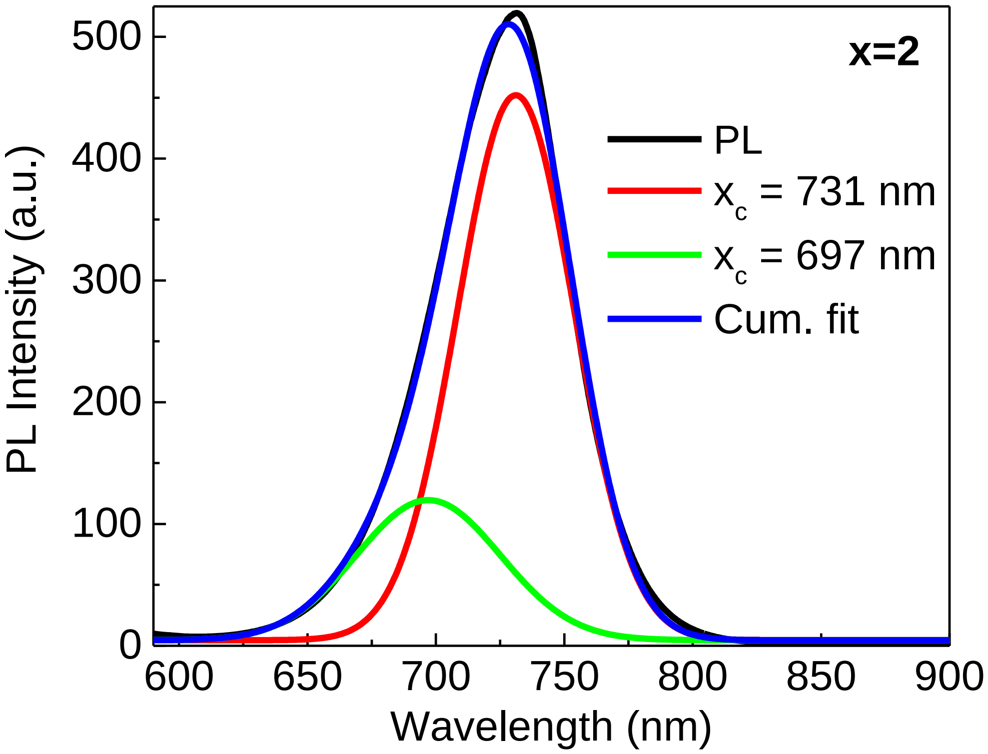

Figure 3.27: PL deconvolution of the $CH_3NH_3PbIBr_2$ perovskite sample

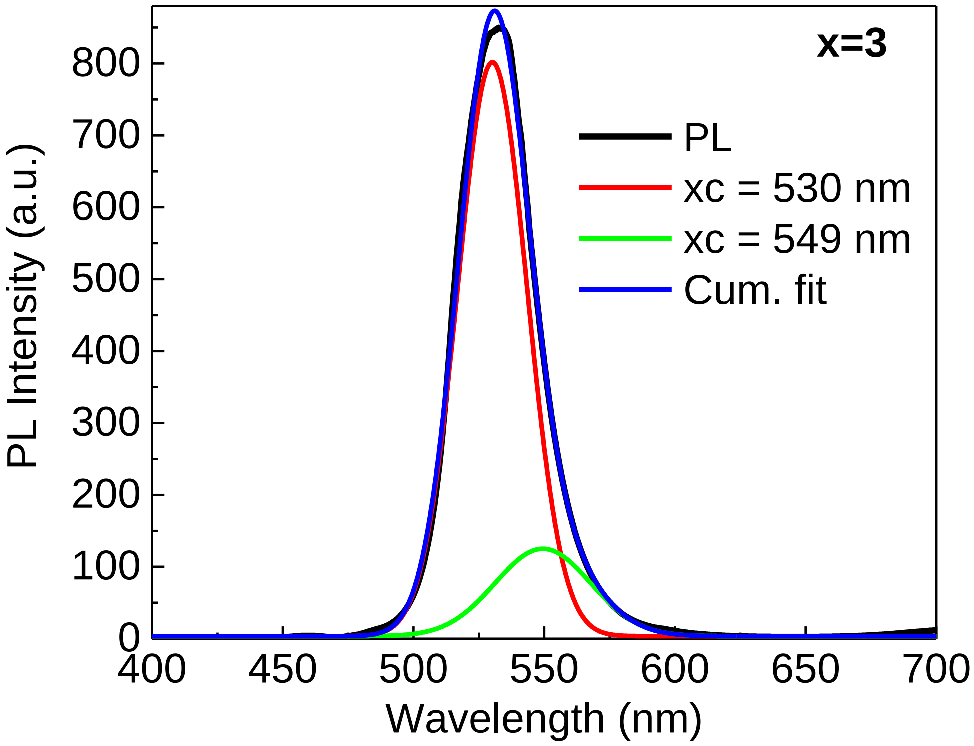

Figure 3.28: PL deconvolution of the $CH_3NH_3PbBr_3$ perovskite sample

CHAPTER 4.

CONCLUSION AND FUTURE LOOK

In this study, bromide-iodide mixed halide perovskite thin films were successfully fabricated on glass substrates by using two and three sources of thermal evaporation system. Five sets of partial bromide substituted perovskite thin films were characterized optically and structurally by using SEM, XRD, UV-Vis and PL techniques. In the literature, there are various bromide-iodide mixed lead halide perovskite studies with supporting and contradictory results [55]. The replication studies supply more evidence to reach the accurate intrinsic properties of this type of perovskites. Most of the mixed halide studies were done by solution process techniques with modifications. To the best of searched knowledge, a bromide-iodide mixed lead halide perovskite in full range by fully evaporation fabrication study has not been published yet. This study gives a chance to compare the results both within the study and with other studies as to put forth the differences between the fabrication techniques.

Thermal co-evaporation technique was examined in different ways by using MAI, MABr, PbI_2, $PbBr_2$ powders as precursors for hybrid lead halide perovskites. Deposition processes demonstrated that MAI/MABr evaporates omnidirectional and its control is mainly based on pressure control. On the other hand, PbI_2/$PbBr_2$ sublimation is unidirectional. The film formation upon the substrate depends on the sublimation speed of the source materials. As a general rule, lower deposition rate gives enough time for the molecules to move the lowest energy positions where they can incorporate to form perovskite. The whole deposition process was controlled by a series of PID and feedback mechanisms. The fine tuning of the deposition parameters makes it available to fabricate perovskites with various contents. For better optical and structural properties, different deposition parameters were tried. Reduced deposition pressure and methanol annealing resulted in larger crystals in general. For band gap tuning process, 0.6 Å/s deposition rate for each source and 3 x 10^{-5} torr deposition pressure were chosen as they gave structurally better perovskites. Methanol annealing was also tested and for 3 x 10^{-5} torr case, it was measured that as deposited sample had larger grains and better crystallinity.

Based on SEM and XRD results, we can claim that pin-hole free perovskite films with various Br/I ratio concentrations were fabricated. It was observed that the bromide content affect the crystallinity and morphology of the perovskite. However, as other studies have also shown, no direct correlation of Br concentration with grain size was observed. The sample of 0.5 Br/I ratio had larger grains than pure I perovskite. For other samples, grain size do not follow the trend. There is no substantial surface morphology change was observed while the grain aggregation increases with more bromide. There were no significant XRD peaks from source materials, indicating pure perovskite formation. Preferential growth in (110) or (100) directions were observed for all Br concentrations. XRD patterns demonstrated regular shift to larger degrees with the increase of bromide content. This also indicates decrease in lattice spacing with smaller Br atoms in perovskite. From FWHM of the (110) peaks, the crystal quality was compared and mixed halide samples had larger values of FWHM, showing mixed halide samples had poorer perovskite formation than pure halide samples. Differences of FWHM values were consistent with the deposition processes as the instabilities during depositions resulted in larger FWHM values.

UV-Vis and PL measurements show the absorption and emission spectra of the mixed halide perovskites. As in XRD patterns, regular shifts were obtained from the results. The optical band gaps range from 1.55 eV to 2.3 eV by the two extreme points. Other samples had 1.65, 1.76, 1.92 eV band gaps. The absorption onsets were steep and linear indicating clear band gaps and lack of trap states. However from PL deconvolution, some phase segregation and poor crystallinity sites are observed as two separate peaks were present. Stokes shift are common and also expected for the missed halide samples as there appears non-uniform mixture of bromide and iodide. It can be concluded that samples showing relatively small crystals by XRD had also large Stokes shift and larger shoulders in PL patterns. The x=1 sample which had very small Stokes shift has appropriate properties for tandem applications with the band gap of 1.65 eV.

In summary, it is demonstrated that $CH_3NH_3I_{3-x}Br_x$ perovskite thin film properties can be tuned by thermal co-evaporation technique. The results showed that bromide substitution affected on the properties and bromide incorporation can be useful for various applications, especially for tandem solar cells. Thermal co-evaporation allows reproducibility and fine-tuning particularly needed by specific properties with stable and fine control of deposition parameters.

Further work on this topic can be continued with detailed characterization such as EDX, XPS, UPS, time dependent PL, etc. Degradation and destructive effects of these techniques must be taken into account and also studied intensely. UPS studies can be used to determine the valance band and conduction band energy positions to better match with transport layers in devices. After optimizing deposition parameters and post-treatment conditions for the best absorber obtained, solar cell fabrication with both conventional and inverted structure can be performed. Deposition pressures smaller than 3 x 10^{-5} torr should be fabricated. As stability is still a major issue with perovskite, effect of bromide inclusion on the stability can also be studied.

REFERENCES

[1] S. Eden. “İklim Krizi ve Yaptırmamak”. Doruk Yay., 2015.

[2] Mitzi D. B., Field C. A, Schlesinger Z., Laibowitz R. B. “Transport, Optical, and Magnetic Properties of the Conducting Halide Perovskite CH3NH3SnI3” J. Solid State Chem. 1995, 114, 159.

[3] Liang K., Mitzi D. B., Prikas M. T. “Synthesis and Characterization of Organic−Inorganic Perovskite Thin Films Prepared Using a Versatile Two-Step Dipping Technique”. Chemistry of Materials 1998, 10, 403.

[4] Hong X., Ishihara T., Nurmikko A. V. “Photoconductivity and Electroluminescence in Lead Iodide Based Natural Quantum-Well Structures”. Solid State Commun. 1992, 84, 657-661

[5] Kagan C. R., Mitzi D. B., Dimitrakopoulos C. D. “Organic-inorganic hybrid materials as semiconducting channels in thin-film field-effect transistors”. Science 1999, 286, 945-947

[6] Green M. A., Jiang Y., Soufiani A. M., Ho-Baillie A. “Optical Properties of Photovoltaic Organic−Inorganic Lead Halide Perovskites”. J. Phys. Chem. Lett. 2015, 6, 4774−4785.

[7] Hattori T., Taira T., Era M., Tsutsui T, Saito S. “Highly Efficient Electroluminescence from a Hetero-structure Device Combined with Emissive Layered-Perovskite and an Electron-Transporting Organic Compound”. Chem. Phys. Lett. 1996, 254, 103 - 108.

[8] Xu C.-Q., Sakakura H., Kondo T., Takeyama S., Miura N., Takahashi Y., Kumata K., Ito R. “Magneto-optical effects of excitons in (C10H21NH3)2PbI4 under high magnetic fields up to 40 T”. Solid State Commun. 1991, 79, 249-253.

[9] Chondroudis K., Mitzi D. B. “Electroluminescence from an Organic−Inorganic Perovskite Incorporating a Quaterthiophene Dye within Lead Halide Perovskite Layers”. Chem. Mater. 1999, 11, 3028.

[10] Era M., Morimoto S., Tsutsui T., Saito, S. “Electroluminescent device using two dimensional semiconductor (C6H5C2H4NH3)2PbI4 as an emitter”. Synth. Met. 1995, 71, 2013–2014.

[11] Evans A., Strezov V., Evans T. J. “Assessment of sustainability indicators for renewable energy technologies”. Renewable and Sustainable Energy Reviews 13 (2009) 1082–1088.

[12] Stranks S. D., Eperon G. E., Grancini G., Menelaou C, Alcocer M. J. P., Leijtens T., et al. “Electron-Hole Diffusion Lengths Exceeding 1 Micrometer in an Organometal Trihalide Perovskite Absorber”. Science. 342 (2013) 341–344.

[13] Green M. A., Ho-Baillie, A., Snaith, H. J. “The emergence of perovskite solar cells”. Nature Photonics 8, 506–514 (2014).

[14] C.C. Stoumpos, C.D. Malliakas, and M.G. Kanatzidis. “Semiconducting tin and lead iodide perovskites with organic cations: phase transitions, high mobility and near-infrared photoluminescent properties”. Inorg. Chem. 52, 9019 (2013).

[15] De Wolf S., Holovsky J., Moon S.-J., Löper P., Niesen B., Ledinsky M., Haug F.-J., Yum J.-H., Ballif C. J. “Organometallic Halide Perovskites: Sharp Optical Absorption Edge and Its Relation to Photovoltaic Performance”. Phys. Chem. Lett. 2014, 5, 1035-1039.

[16] Stranks S. D., Eperon G. E., Grancini G., Menelaou C., Alcocer M. J. P., Leijtens T., Herz L. M., Petrozza A., Snaith H. “Electron-Hole Diffusion Lengths Exceeding 1 Micrometer in an Organometal Trihalide Perovskite Absorber”. J. Science 2013, 342, 341-344.

[17] de Quilettes D. W., Vorpahl S. M., Stranks S. D., Nagaoka H., Eperon G. E., Ziffer M. E., Snaith H. J., Ginger D. S. “Impact of microstructure on local carrier lifetime in perovskite solar cells”. Science 2015, 348, 683-686.

[18] [e] Xing G., Mathews N., Sun S., Lim S. S., Lam Y. M., Grätzel M., Mhaisalkar S., Sum T. C. “Long-Range Balanced Electron- and Hole-Transport Lengths in Organic-Inorganic CH3NH3PbI3”. Science 2013, 342, 344-347.

[19] Dong Q., Fang Y., Shao Y., Mulligan P., Qiu J., Cao L., Huang J. “Electron-hole diffusion lengths > 175 µm in solution-grown CH3NH3PbI3 single crystals”. Science 2015, 347, 967-970.

[20] Stranks S. D., Burlakov V. M., Leijtens T., Ball J. M., Goriely A., Snaith H. J. “Recombination Kinetics in Organic-Inorganic Perovskites: Excitons, Free Charge, and Subgap States”. Phys. Rev. Appl. 2014, 2, 034007.

[21] Jeon N. J., Noh J. H., Yang W. S., Kim Y. C., Ryu S., Seo J., Seok S. I. “Compositional engineering of perovskite materials for high-performance solar cells”. Nature 2015, 517, 476-480.

[22]Green M. A., Emery K., Hishikawa Y., Warta W., Dunlop E. D. “Solar cell efficiency tables (Version 45)”. Prog. Photovoltaics 2015, 23, 1-9.

[23] Löper P., Moon S.-J., de Nicolas S. M., Niesen B., Ledinsky M., Nicolay S., Bailat J., Yum J.-H., Wolf S. D., Ballif C. “Organic–inorganic halide perovskite/crystalline silicon four-terminal tandem solar cells”. Phys. Chem. Chem. Phys. 2014, 17, 1619-1629.

[24] Mailoa J. P., Bailie C. D., Johlin E. C., Hoke E. T., Akey A. J., Nguyen W. H., McGehee M. D., Buonassisi T. “A 2-terminal perovskite/silicon multijunction solar cell enabled by a silicon tunnel junction”. Appl. Phys. Lett. 2015, 106, 121105.

[25] Bailie C. D., Christoforo M. G., Mailoa J. P., Bowring A. R., Unger E. L., Nguyen W. H., Burschka J., Pellet N., Lee J. Z., Gratzel M., Noufi R., Buonassisi T., Salleo A., McGehee M. D. “Semi-transparent perovskite solar cells for tandems with silicon and CIGS”. Energy Environ. Sci. 2015, 8, 956-963.

[26] Kranz L., Abate A., Feurer T., Fu F., Avancini E., Löckinger J., Reinhard P., Zakeeruddin S. M., Gratzel M., Buecheler S., Tiwari A. N. “High-Efficiency Polycrystalline Thin Film Tandem Solar Cells”. J. Phys. Chem. Lett. 2015, 6, 2676-2681

[27] Bailie C. D., McGehee M. D. “High-efficiency tandem perovskite solar cells”. MRS Bulletİn Volume 40, August 2015.

[28] Yang W. S., Noh J. H.; Jeon N. J., Kim Y. C., Ryu S., Seo J., Seok S. I. “High-Performance Photovoltaic Perovskite Layers Fabricated Through Intramolecular Exchange”. Science 2015, 348, 1234-1237.

[29] F. Hao, C. C. Stoumpos, D. H. Cao, R. P. H. Chang and M. G. Kanatzidis “Lead-free solid-state organic–inorganic halide perovskite solar cells”. Nat. Photonics, vol. 8, no. 6, pp. 489–494, May 2014.

[30] Fang, Y., Dong, Q., Shao, Y., Yuan, Y., Huang, J. “Highly narrowband perovskite single-crystal photodetectors enabled by surface-charge recombination”. Nat. Photonics 2015, 9, 679−686.

[31]. L. Huang and W.R.L. Lambrecht. “Electronic band structure, phonons,

and exciton binding energies of halide perovskites CsSnCl3, CsSnBr3, and CsSnI3”. Phys. Rev. B 88, 165203 (2013).

[32] Noh J. H., Im S. H., Heo J. H., Mandal T. N., Il Seok S. “Chemical Management for Colorful, Efficient, and Stable Inorganic–Organic Hybrid Nanostructured Solar Cells”. Nano Lett. 13, 1764-1769 (2013).

[33] G.E. Eperon, V.M. Burlakov, A. Goriely, and H.J. Snaith. “Neutral color semitransparent micro-structured perovskite solar cells”. ACS Nano 8, 591 (2014).

[34] K. Tvingstedt, O. Malinkiewicz, A. Baumann, C. Deibel, H. J. Snaith, V. Dyakonov, H. J. Bolink. “Radiative efficiency of lead iodide based perovskite solar cells”. Scientific Reports 4, Article number: 6071 (2014).

[35] Elliott, R. Intensity of Optical Absorption by Excitons. Phys. Rev. 1957, 108, 1384−1389.

[36] W. Wang, Y. Li, X. Wang, Y. Lv, S. Wang, K. Wang, Y. Shi, L. Xiao, Z. Chen, Q. Gong. "Dynamical co-existence of excitons and free carriers in perovskite probed by density-resolved fluorescent spectroscopic method". arXiv:1608.03529.

[37] L. Q. Phuong, Y. Yamada, M. Nagai, N. Maruyama, A. Wakamiya, Y. Kanemitsu. "Free Carriers versus Excitons in CH3NH3PbI3 Perovskite Thin Films at Low Temperatures: Charge Transfer from the Orthorhombic Phase to the Tetragonal Phase". J. Phys. Chem. Lett., 2016, 7 (13), pp 2316–2321.

[38] Tan Z.-K., Moghaddam R. S., Lai M. L., Docampo P., Higler R., Deschler F., Price M., Sadhanala A., Pazos L. M., Credgington D., Hanusch F., Bein T., Snaith H. J., Friend R. H. "Bright light-emitting diodes based on organometal halide perovskite". Nat. Nanotechnol. 2014, 9, 687-692.

[39] Ning Z., Gong X., Comin R., Walters G., Fan F., Voznyy O., Yassitepe E., Buin A., Hoogland S., Sargent E. H. "Quantum-dot-in-perovskite solids". Nature 2015, 523, 324-328.

[40] Saba M., Cadelano M., Marongiu D., Chen F., Sarritzu V., Sestu N., Figus C., Aresti M., Piras R., Geddo Lehmann A., Cannas C., Musinu A., Quochi F., Mura A., Bongiovanni G. "Correlated electron–hole plasma in organometal perovskites". Nat. Commun. 2014, 5, 5049.

[41] T. M. Brenner, D. A. Egger, L. Kronik, G. Hodes and D. Cahen. "Hybrid organic–inorganic perovskites: low-cost semiconductors with intriguing charge-transport properties". Nature Reviews Materials, Vol. 1, Issue 1, pp. 15007 (2016).

[42] Mosconi E., Azpiroz J. M., De Angelis F. "Ab Initio Molecular Dynamics Simulations of MAPbI3 Perovskite Degradation by Water". Chem. Mater. 2015, 27, 4885-4892.

[43] Conings B., Drijkoningen J., Gauquelin N., Babayigit A., D'Haen J., D'Olieslaeger L., Ethirajan A., Verbeeck J., Manca J., Mosconi E., et al. "Intrinsic

Thermal Instability of Methylammonium Lead Trihalide Perovskite”. Adv. Energy Mater. 2015, 5, 1500477

[44] Ledinsky M., Löper P., Niesen B., et al. “Raman Spectroscopy of Organic-Inorganic Halide Perovskites”. J. Phys. Chem. Lett. 2015, 6, 401-406.

[45] Eames C., Frost J. M., Barnes P. R. F., O’Regan B. C., Walsh A., Islam M. S. “Ionic Transport in Hybrid Lead Iodide Perovskite Solar Cells”. Nat. Commun. 2015, 6, 7497.

[46] Mei, A.; Li, X.; Liu, L.; Ku, Z.; Liu, T.; Rong, Y.; Xu, M.; Hu, M.; Chen, J.; Yang, Y.; Gratzel, M.; Han, H. “A hole-conductor-free, fully printable mesoscopic perovskite solar cell with high stability”. Science 2014, 345, 295−298.

[47] T. A. Berhe, W.-N. Su, C.-H. Chen, C.-J. Pan, J.-H. Cheng, H.-M. Chen, M.-C. Tsai, L.-Y. Chen, A. A. Dubale and B.-J. Hwang. “Organometal halide perovskite solar cells: degradation and stability”. Energy Environ. Sci., 2016,9, 323-356.

[48] S. Brittman, G. W. P. Adhyaksa, and E. Christian Garnett. “The expanding world of hybrid perovskites: materials properties and emerging applications”. MRS Communications (2015), 5, 7–26

[49] S. Aharon, S. Gamliel, B. E. Cohen and L. Etgar. “Depletion region effect of highly efficient hole conductor free CH3NH3PbI3 perovskite solar cells”. Phys. Chem. Chem. Phys., 2014, 16, 10512–10518.

[50] M. M. Lee, J. Teuscher, T. Miyasaka, T. N. Murakami and H. J. Snaith. “Efficient Hybrid Solar Cells Based on Meso-Superstructured Organometal Halide Perovskites”. Science, 2012, 338, 643–647.

[51] Hoke E. T., Slotcavage D. J., Dohner E. R., Bowring A. R., Karunadasa H. I., McGehee M. D. “Reversible Photo-Induced Trap Formation in Mixed-Halide Hybrid Perovskites for Photovoltaics”. Chem. Sci. 2015, 6, 613-6177.

[52] D. A. Egger, E. Edri, D. Cahen, G. Hodes. “Perovskite Solar Cells: Do We Know What We Do Not Know?”. J. Phys. Chem. Lett. 2015, 6, 279−282.

[53] E. T. Hoke, D. J. Slotcavage, E. R. Dohner, A. R. Bowring, H. I. Karunadasa and M. D. McGehee. “Reversible photo-induced trap formation in mixed-halide hybrid perovskites for photovoltaics”. Chem. Sci., 2015, 6, 613–617.

[54] A. Sadhanala, F. Deschler, T.H. Thomas, E. Dutton, K.C. Goedel, F.C. Hanusch, M.L. Lai, U. Steiner, T. Bein, P. Docampo, D. Cahen, and

R.H. Friend. “Preparation of single-phase films of CH3NH3Pb(I1-xBrx)3

with sharp optical band edges”. J. Phys. Chem. Lett. 5, 2501 (2014).

[55] H.-S. Kim, J.-Y. Seo, N.-G. Park. “Material and Device Stability in Perovskite Solar Cells”. ChemSusChem 2016, 9, 2528.

[56] T. Miyasaka. “Perovskite Photovoltaics: Rare Functions of Organo Lead Halide in Solar Cells and Optoelectronic Devices”. Chem.Lett. 2015, 44, 720–729.

[57] A. Babayigit, A. Ethirajan, M. Muller, B. Conings. “Toxicity of organometal halide perovskite solar cells”. Nature Materials 15, 247–251 (2016).

[58] Docampo P, Bein T. “A Long-Term View on Perovskite Optoelectronics”. Acc Chem Res. 2016 Feb 16; 49(2):339-46.

[59] T. Miyasaka. “Perovskite Photovoltaics: Rare Functions of Organo Lead Halide in Solar Cells and Optoelectronic Devices”. Chem. Lett. 2015, 44, 720–729.

[60] Bremner S. P., Levy M. Y., Honsberg C. B. “Analysis of tandem solar cell efficiencies under AM1.5G spectrum using a rapid flux calculation method”. Prog. Photovoltaics 2008, 16, 225-233.

[61] Essig S., Ward S., Steiner M. A., Friedman D. J., Geisz J. F., Stradins P., Young D. L. “Progress Towards a 30% Efficient GaInP/Si Tandem Solar Cell”. Energy Procedia 2015, 77, 464-469.

[62] Liang K, Mitzi D. B, Prikas M. T. (1998) “Synthesis and characterization of organic–inorganic perovskite thin films prepared using a versatile two-step dipping technique”. Chem Mater 10:403–411

[63] C. M. Sutter-Fella, Y. Li, M. Amani, J. W. Ager III, F. M. Toma, E. Yablonovitch, I. D. Sharp, and A. Javey. "High Photoluminescence Quantum Yield in Band Gap Tunable Bromide Containing Mixed Halide Perovskites". Nano Lett. 2016, 16, 800−806

[64] G. E. Eperon, V. M. Burlakov, P. Docampo, A. Goriely, H. J. Snaith. "Morphological Control for High Performance, Solution-Processed Planar Heterojunction Perovskite Solar Cells". Adv. Funct. Mater. 2014, 24, 151-157

[65] C.-Y. Chang, C.-Y. Chu, Y.-C. Huang, C.-W. Huang, S.-Y. Chang, C.-A. Chen, C.-Y. Chao, W.-F. Su. "Tuning perovskite morphology by polymer additive for high efficiency solar cell." ACS Appl. Mater. Interfaces 2015, 7, 4955.

[66] C.-C. Chueh, C.-Y. Liao, F. Zuo, S. T. Williams, P.-W. Liang, A. K. Y. Jen, J. "The roles of alkyl halide additives in enhancing perovskite solar cell performance". Mater. Chem. A 2015, 3, 9058.

[67] J. H. Heo, D. H. Song, S. H. Im, "Planar CH3NH3PbBr3 Hybrid Solar Cells with 10.4% Power Conversion Efficiency, Fabricated by Controlled Crystallization in the Spin-Coating Process". Adv. Mater. 2014, 26, 8179-8183.

[68] C. Sun, Q. Xue, Z. Hu, Z. Chen, F. Huang, H.-L. Yip, Y. Cao. "Phosphonium Halides as Both Processing Additives and Interfacial Modifiers for High Performance Planar-Heterojunction Perovskite Solar Cells". Small 2015.

[69] Y. Chen, Y. Zhao, Z. Liang. "Non-Thermal Annealing Fabrication of Efficient Planar Perovskite Solar Cells with Inclusion of NH4Cl" Chem. Mater. 2015, 27, 1448.

[70] G. E. Eperon, S. D. Stranks, C. Menelaou, M. B. Johnston, L. M. Herz, H. J. Snaith. "Formamidinium lead trihalide: a broadly tunable perovskite for efficient planar heterojunction solar cells". Energy Environ. Sci. 2014, 7, 982.

[71] X. Song, W. Wang, P. Sun, W. Ma, Z.-K. Chen. "Additive to regulate the perovskite crystal film growth in planar heterojunction solar cells". Appl. Phys. Lett. 2015, 106, 033901.

[72] P.-W. Liang, C.-Y. Liao, C.-C. Chueh, F. Zuo, S. T. Williams, X.-K. Xin, J. Lin, A. K.Y. Jen, Adv. Mater. 2014, 26, 3748.

[73] C. Zuo, L. Ding. “An 80.11% FF record achieved for perovskite solar cells by using the NH4Cl additive”. Nanoscale 2014, 6, 9935.

[74] N. J. Jeon, J. H. Noh, Y. C. Kim, W. S. Yang, S. Ryu and S. I. Seok. “Solvent engineering for high-performance inorganic-organic hybrid perovskite solar cells”. Nat. Mater., 2014, 13, 897-903.

[75] D. Shen, X. Yu, X. Cai, M. Peng, Y. Ma, X. Su, L. Xiao, D. Zou. “Understanding the solvent-assisted crystallization mechanism inherent in efficient organic–inorganic halide perovskite solar cells”. J. Mater. Chem. A 2014, 2, 20454.

[76] H.-B. Kim, H. Choi, J. Jeong, S. Kim, B. Walker, S. Song, J. Y. Kim. “Mixed solvents for the optimization of morphology in solution-processed, inverted-type perovskite/fullerene hybrid solar cells”. Nanoscale 2014, 6, 6679.

[77] S. Paek, N. Cho, H. Choi, H. Jeong, J. S. Lim, J.-Y. Hwang, J. K. Lee, J. Ko. “Improved External Quantum Efficiency from Solution-Processed (CH3NH3)PbI3 Perovskite/PC71BM Planar Heterojunction for High Efficiency Hybrid Solar Cells”. J. Phys. Chem. C 2014, 118, 25899

[78] Liang, P.-W.; Liao, C.-Y.; Chueh, C.-C.; Zuo, F.; Williams, S. T.; Xin, X.-K.; Lin, J.; Jen, A. K. Y. “Additive Enhanced Crystallization of Solution-Processed Perovskite for Highly Efficient Planar-Heterojunction Solar Cells”. Adv. Mat. 2014, 26, 3748−3754.

[79] Saliba, M.; Tan, K. W.; Sai, H.; Moore, D. T.; Scott, T.; Zhang, W.; Estroff, L. A.; Wiesner, U.; Snaith, H. J. “Influence of Thermal Processing Protocol upon the Crystallization and Photovoltaic Performance of Organic−Inorganic Lead Trihalide Perovskites”. J. Phys. Chem. C 2014, 118, 17171−17177.

[80] Zhang, W.; Saliba, M.; Moore, D. T.; Pathak, S. K.; Hörantner, M. T.; Stergiopoulos, T.; Stranks, S. D.; Eperon, G. E.; AlexanderWebber, J. A.; Abate, A.; Sadhanala, A.; Yao, S.; Chen, Y.; Friend, R. H.; Estroff, L. A.; Wiesner, U.; Snaith,

H. J. "Ultrasmooth organic−inorganic perovskite thin-film formation and crystallization for efficient planar heterojunction solar cells". Nat. Comm. 2015, 6, 6142.

[81] Leijtens, T.; Lauber, B.; Eperon, G. E.; Stranks, S. D.; Snaith, H. J. "The Importance of Perovskite Pore Filling in Organometal Mixed Halide Sensitized TiO2-Based Solar Cells". J. Phys. Chem. Lett. 2014, 5, 1096−1102.

[82] Liu M, Johnston M. B., Snaith H. J. (2013) "Efficient planar heterojunction perovskite solar cells by vapour deposition". Nature 501:395–398.

[83] Wang Q., Chen H., Liu G., Wang L. "Control of organic–inorganic halide perovskites in solid-state solar cells: a perspective". Sci. Bull. (2015) 60(4):405–418.

[84] C. Momblona, O. Malinkiewicz, C. Roldán-Carmona, A. Soriano, L. Gil-Escrig, E. Bandiello, M. Scheepers, E. Edri, H. J. Bolink. "Efficient methylammonium lead iodide perovskite solar cells with active layers from 300 to 900 nm". APL Mater. 2014, 2, 081504.

[85] Cristina Roldán-Carmona, Olga Malinkiewicza, Alejandra Sorianoa, Guillermo Mínguez Espallargasa, Ana Garciac, Patrick Reineckec, Thomas Kroyerc, M. Ibrahim Dare, Mohammad Khaja Nazeeruddine and Henk J. Bolink. "Flexible high efficiency perovskite solar cells". Energy Environ. Sci., 2014,7, 994-997.

[86] Liu C., Wang K., Yi C., Shi X., Smith A. W., Gong X. and Heeger A. J. (2016). "Efficient Perovskite Hybrid Photovoltaics via Alcohol-Vapor Annealing Treatment". Adv. Funct. Mater., 26: 101–110.

[87] J. Liu, C. Gao, X. He, Q. Ye, L. Ouyang, D. Zhuang, C. Liao, J. Mei, and W. Lau. "Improved Crystallization of Perovskite Films by Optimized Solvent Annealing for High Efficiency Solar Cell". ACS Appl. Mater. Interfaces, 2015, 7 (43), pp 24008–24015.

[88] Dong Cui, Zhou Yang, Dong Yang, Xiaodong Ren, Yucheng Liu, Qingbo Wei, Haibo Fan, Jinghui Zeng and Shengzhong (Frank) Liu. "Color-Tuned Perovskite

Films Prepared for Efficient Solar Cell Applications”. J. Phys. Chem. C 2016, 120, 42−47.

[89] R. Gottesman and A. Zaban. “Perovskites for Photovoltaics in the Spotlight: Photoinduced Physical Changes and Their Implications”. Acc. Chem. Res., 2016, 49 (2), pp 320–329.

[90] Açık E. “Poly(Lactic Acid) Based Nanocomposites: Mechanical, Thermal And Rheological Properties And Morphology”. PhD. Thesis, METU, 2014.

[91] "Transmission and Scanning Electron Microscopy,". Available online at: www.expertsmind.com/topic/looking-at-microbes/transmission-and-scanning-electron-microscopy-92282.aspx, last visited on August 2016.

[92] Hanusch C. A. Fabian. “Solution Processed Perovskite Solar Cells. Dissertation for Doctorate Degree”. The Faculty of Chemistry and Pharmacy, The Ludwig Maximilian University of Munich, 2015.

[93] B. D. Cullity, “Elements of X-Ray Diffraction “, Addison-Wesley, Second Edition, 1978.

[94] Yerci S. “Spectroscopic Characterization Of Semiconductor Nanocrystals”. M.S. Thesis, METU, 2007.

[95] Nogay, G. “Effect Of Deposition Parameters On Silicon Layers Transition From Amorphous Phase To Micro/Nano-Crystalline Phase In Different Deposition Techniques”, M.S. Thesis, METU, 2013.

[96] Seyhan A., “Photoluminescence Spectroscopy of Cds and GaSe”, M.S. Thesis, METU, 2003.

[97] B. Park, B. Philippe, S. M. Jain, X. Zhang, T. Edvinsson, H. Rensmo, B. Zietza and G. Boschloo. “Chemical engineering of methylammonium lead iodide/bromide perovskites: tuning of optoelectronic properties and photovoltaic performance”. J. Mater. Chem. A, 2015, 3, 21760.

[98] Chen Q., Zhou H., Hong Z., Luo S., Duan H.-S., Wang H.-H., Liu Y., Li G., Yang Y. "Planar heterojunction perovskite solar cell via vapor-assisted solution process". J. Am. Chem. Soc. 136, 622–625 (2014).

[99] Burschka J., Pellet N., Moon S. J., Humphry-Baker R., Gao P., Nazeeruddin M. K. and Grätzel M. "Sequential deposition as a route to high-performance perovskite-sensitized solar cells". Nature 499, 316–319 (2013).

[100] Sun S., Salim, T., Mathewa N., Duchamp M., Boothroyd C., Xing G., Sum T. C. and Lam Y. M. "The origin of high efficiency in low-temperature solution-processable bilayer organometal halide hybrid solar cells". Energy Environ. Sci. 7, 399–407 (2014).

[101] B. Park, S. M. Jain, X. Zhang, A. Hagfeldt, G. Boschloo, and T. Edvinsson. "Resonance Raman and Excitation Energy Dependent Charge Transfer Mechanism in Halide-Substituted Hybrid Perovskite Solar Cells". ACS. Nano, Vol. 9, No. 2, 2088-2101 (2015).

[102] M. I. Dar, M. Abdi-Jalebi, N. Arora, T. Moehl, M.Grätzel, and M. K. Nazeeruddin. "Understanding the Impact of Bromide on the Photovoltaic Performance of CH3NH3PbI3 Solar Cells". Adv. Mat., Vol. 27, Iss. 44, 7221–7228, 2015.

[103] C. Li, J. Wei, M. Sato, H. Koike, Z. Xie, Y. Li, K. Kanai, S. Kera, N. Ueno, and J. Tang. "Halide-Substituted Electronic Properties of Organometal Halide Perovskite Films: Direct and Inverse Photoemission Studies". ACS Appl. Mater. Interfaces, 2016, 8 (18), pp 11526–11531

[104] S. A. Kulkarni, T. Baikie, P. P. Boix, N. Yantara, N. Mathews and S. Mhaisalkar. "Band-gap tuning of lead halide perovskites using a sequential deposition process". J. Mater. Chem. A, 2014, 2, 9221.

[105] Im J.-H., Lee C.-R., Lee J.-W, Park, S.-W. & Park, N.-G. "6.5% efficient perovskite quantum-dot-sensitized solar cell". Nanoscale 3, 4088–4093 (2011).

[106] Kojima A., Teshima K., Shirai Y. & Miyasaka T. "Organometal halide perovskites as visible-light sensitizers for photovoltaics cells". J. Am. Chem. Soc. 131, 6050–6051 (2009).

[107] Baikie T., Fang Y., Kadro J. M., Schreyer M., Wei F., Mhaisalkar S. G. Graetzel M. and White T. J. "Synthesis and crystal chemistry of the hybrid perovskite (CH3NH3)PbI3 for solid-state sensitised solar cell applications". J. Mater. Chem. A 1, 5628–5641 (2013).

[108] B. Suarez, V. Gonzalez-Pedro, T. S. Ripolles, R. S. Sanchez, L. Otero, I. Mora-Sero. "Recombination Study of Combined Halides (Cl, Br, I) Perovskite Solar Cells". J. Phys. Chem. Lett. 2014, 5, 1628−1635.

[109] W. Huang, J. S. Manser, P. V. Kamat, and S. Ptasinska. "Evolution of Chemical Composition, Morphology, and Photovoltaic Efficiency of CH3NH3PbI3 Perovskite under Ambient Conditions". Chem. Mater., 2016, 28 (1), pp 303–311.

[110] R. J. Hill. "Energy-gap variations in semiconductor alloys". Phys. C: Solid State Phys. 7 (1974) 521–526.

[111] L. Atourki, E. Vega, B. Marí, M. Mollar, H. A. Ahsaine, K. Bouabid, A. Ihlal. "Role of the chemical substitution on the structural and luminescence properties of the mixed halide perovskite thin MAPbI3−xBrx (0≤x≤1) films". Applied Surface Science 371 (2016) 112–117.

[112] A. A. El-Shazly, M. M. H. El-Naby, M. A. Kenawy, M. M. El-Nahass, H. T. El-Shair, A. M. Ebrahim. "Optical properties of ternary ZnSxSe1-x polycrystalline thin films". Appl. Phys. A: Mater. Sci. Process 36 (1985) 51–53.

[113] M. Wang, G. T. Fei, Y. G. Zhang, M. G. Kong, L. D. Zhang. "Tunable and predetermined band gap emissions in alloyed ZnSxSe1 − x nanowires". Adv. Mater. 19 (2007) 4491–4494.

[114] F. Deschler, M. Price, S. Pathak, L.E. Klintberg, D. Jarausch, R. Higler, S. Hu, T. Leijtens, S.D. Stranks, H.J. Snaith, M. Atatu, R.T. Phillips, and R.H. Friend. "High photoluminescence efficiency and optically pumped lasing in solution-

processed mixed halide perovskite semiconductors". J. Phys. Chem. Lett. 5, 1421 (2014).

[115] M. Saba, M. Cadelano, D. Marongiu, F. Chen, V. Sarritzu, N. Sestu, C. Figus, M. Aresti, R. Piras, A. Geddo Lehmann, C. Cannas, A. Musinu, F. Quochi, A. Mura, and G. Bongiovanni: "Correlated electronhole plasma in organometal perovskites". Nat. Commun. 5, 5049 (2014)

[116] N.K. Noel, A. Abate, S.D. Stranks, E.S. Parrott, V.M. Burlakov, A. Goriely, H.J. Snaith, and N.E.T. Al. "Enhanced photoluminescence and solar cell performance via lewis base passivation of organic-inorganic lead halide perovskites". ACS Nano 8, 9815 (2014).

[117] S.D. Stranks, V.M. Burlakov, T. Leijtens, J.M. Ball, A. Goriely, and

H.J. Snaith: "Recombination kinetics in organic-inorganic perovskites: excitons, free charge, and subgap states". Phys. Rev. Appl. 2, 034007 (2014).

[118] A. Sadhanala, F. Deschler, T.H. Thomas, S.E. Dutton, K.C. Goedel, F.C. Hanusch, M.L. Lai, U. Steiner, T. Bein, P. Docampo, D. Cahen, R.H. Friend, Preparation of single phase films of CH3NH3 Pb(I1 − xBrx)3 with sharp optical band edges, J. Phys. Chem.Lett. 5 (2014) 2501–2505.

[119] H.L. Hsu, C.C. Chang, C.P. Chen, B.H. Jiang, R.J. Jeng, C.H. Cheng. "High-performance and high-durability perovskite photovoltaic devices prepared using ethylammonium iodide as an additive". J. Mater. Chem. A 3 (2015) 9271–9277.

[120] P. Fedeli, F. Gazza, D. Calestani, P. Ferro, T. Besagni, A. Zappettini, G. Calestani, E. Marchi, P. Ceroni, R. Mosca. "Influence Of The Synthetic Procedures On The Structural And Optical Properties Of Mixed-Halide (Br, I) Perovskite Film." J. Phys. Chem. C 119 (2015) 21304–21313.